

## **Seafloor geodetic constraints on interplate coupling of the Nankai Trough megathrust zone**

Yusuke Yokota<sup>1</sup>, Tadashi Ishikawa<sup>1</sup>, Shun-ichi Watanabe<sup>1</sup>, Toshiharu Tashiro<sup>1</sup> and Akira Asada<sup>2</sup>

<sup>1</sup>Hydrographic and Oceanographic Department, Japan Coast Guard, 2-5-18, Aomi, Koto-ku, Tokyo 135-0064, Japan (eisei@jodc.go.jp)

<sup>2</sup>Institute of Industrial Science, University of Tokyo, 4-6-1 Komaba, Meguro-ku, Tokyo 153-8505, Japan (asada@iis.u-tokyo.ac.jp)

**Interplate megathrust earthquakes have inflicted catastrophic damage on human society. An extremely hazardous megathrust earthquake is predicted to occur along the Nankai Trough off southwestern Japan, an economically active and densely populated area with historical records of megathrust earthquakes<sup>1-5</sup>. Megathrust earthquakes are the result of a plate subduction mechanism and occur at interplate slip-deficit (or coupling) regions<sup>6-7</sup>. Many past studies have attempted to capture slip-deficit rate (SDR) distributions for assessing future earthquake disasters<sup>8-10</sup>. However, they could not capture a total view of the megathrust earthquake source region because they had no seafloor geodetic data. The Hydrographic and Oceanographic Department of the Japan Coast Guard (JHOD) has been developing a highly precise and sustainable seafloor geodetic observation network<sup>11</sup> deployed in this subduction zone to broadly obtain direct information related to offshore SDR. Here, we present seafloor geodetic observation data and an offshore interplate SDR distribution model. Our data suggests that most offshore regions in this subduction zone have positive SDRs. Specifically, our observations indicate previously unknown high-SDR regions that are important for tsunami disaster mitigation and low-SDR regions that are consistent with distributions of shallow slow earthquakes and subducting seamounts. This is the first direct evidence suggesting that coupling conditions are related to these seismological and geological phenomena. These observations provide new fundamental information for inferring megathrust earthquake scenarios and interpreting research on the Nankai Trough subduction zone.**

Recurring interplate megathrust earthquakes have occurred along the Nankai Trough subduction zone between the Philippine Sea plate and the Amur plate, and the next earthquake is predicted to occur in the near future<sup>1-5</sup>. This subduction zone is frequently discussed in terms of segmented source regions called the Nankaido, Tonankai and Tokai regions, and M8-class earthquakes in these segments are described in the past 300 years of historical records<sup>2</sup> (the 1707 Hōei, 1854 Ansei-I, Ansei-II, 1944 Tonankai and 1946 Nankaido earthquakes). Up to M9-class earthquakes are believed to have occurred along each segment<sup>5</sup>.

Since megathrust earthquakes are driven by accumulated interplate slip-deficit, these historical earthquakes were believed to occur on an interplate boundary with a high SDR<sup>6-7</sup>. To assess the scale of future earthquakes and tsunamis, it is therefore necessary to grasp the whole interplate SDR distribution. While many geodetic approaches have been attempted to obtain this information for the Nankai Trough, they have not been successful. This is because the previous geodetic observation network is biased to land areas and cannot capture total geodetic information on the seafloor above the interplate boundary<sup>8-10</sup>. Although small-scale seafloor geodetic observations have been carried out<sup>12</sup>, observations were limited to only around the Kumano-nada region.

Accordingly, over the past decade we have taken a new approach to obtaining total seafloor geodetic information by means of a broad-scale seafloor observation network using the Global Positioning System and Acoustic ranging combination (GPS-A) technique<sup>11,13-14</sup>. The precision and frequency of our GPS-A observations have been improved by original developments since 2000 and are among the highest standards in the world. Our GPS-A technique is described in the Methods section and Extended Data Fig. 1.

We observe fifteen seafloor sites in a wide seafloor region along the Nankai Trough (Fig. 1). Six sites were established before the 2011 Tohoku-oki earthquake. Since the results of these sites were insufficient to expose a total image of interplate SDR<sup>15</sup>, nine new sites were deployed after 2011.

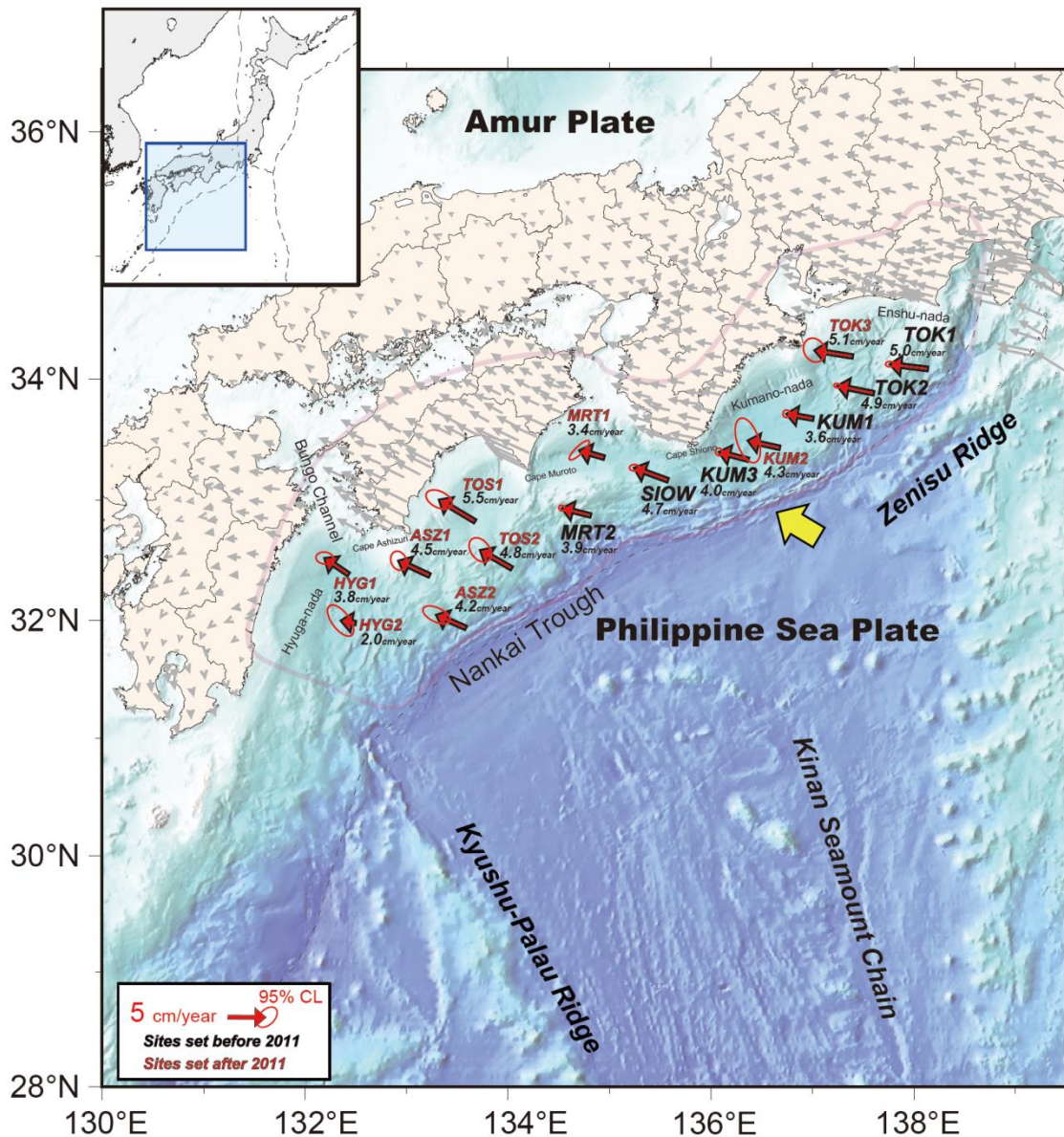
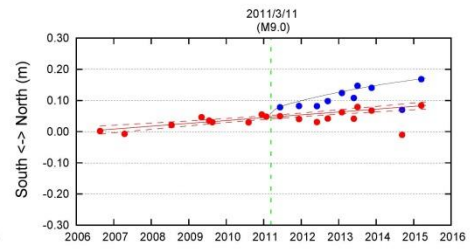
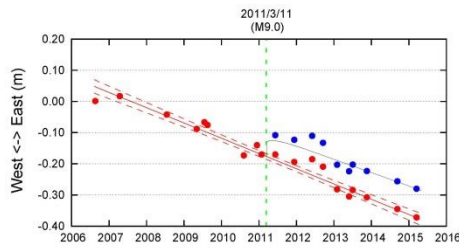


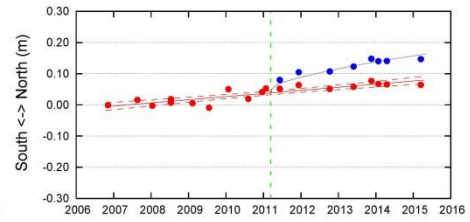
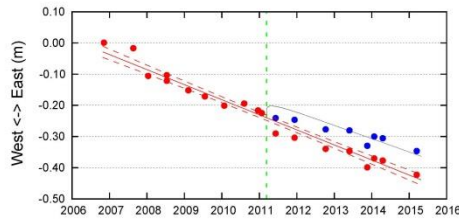
**Fig. 1 | Seafloor velocity field from seafloor geodetic observations at fifteen seafloor sites along the Nankai Trough.**

Seafloor velocity vectors are shown by red arrows. Each ellipse indicates the 95 % confidence level. The onshore velocity vectors are calculated for the period from March 2006 to December 2009 using GEONET stations and shown by light-gray arrows. Yellow arrow indicates the convergence rate (6.5 cm/year) of the Philippine Sea plate under the Amur plate calculated using the MORVEL model<sup>17</sup>. Purple region shows the maximum source region provided as the worst case scenario by the Central Disaster Management Council of the Japanese Government<sup>5</sup>. Seafloor topography was based on J-EGG500 of the Japan Oceanographic Data Center (JODC) of the JHOD.

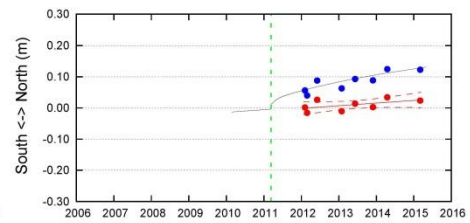
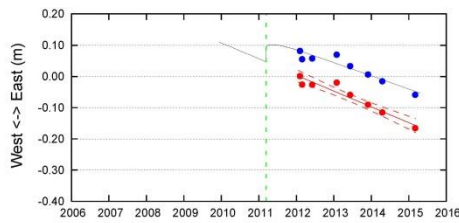
(1) TOK1



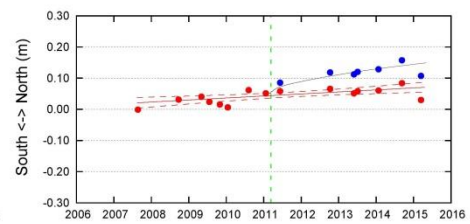
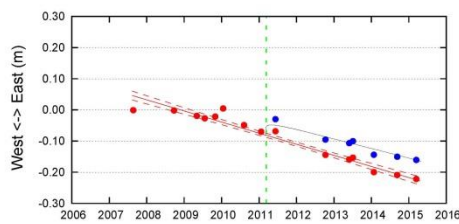
(2) TOK2



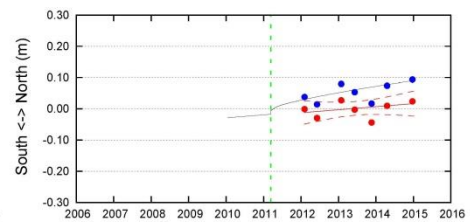
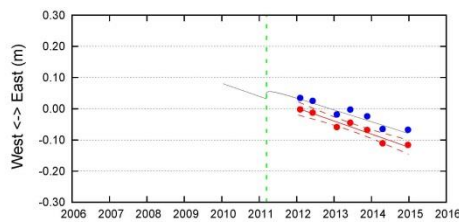
(3) TOK3



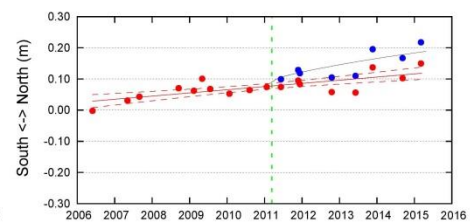
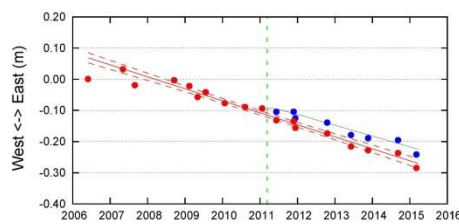
(4) KUM1



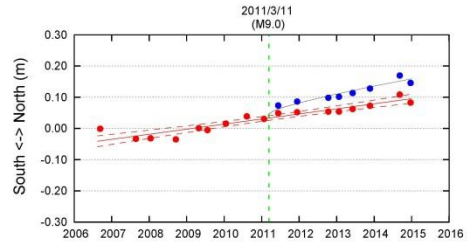
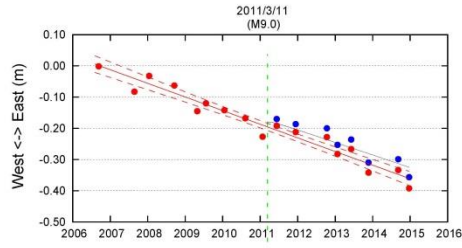
(5) KUM2



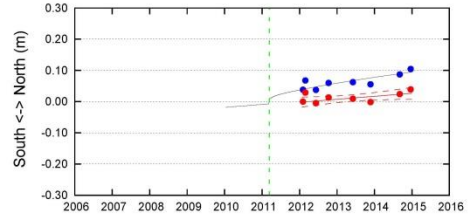
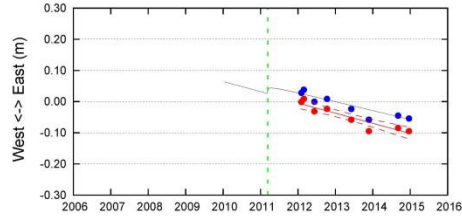
(6) KUM3



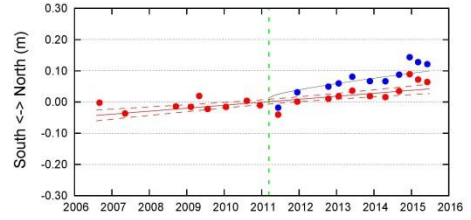
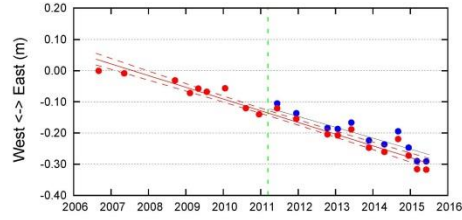
(7) SIOW



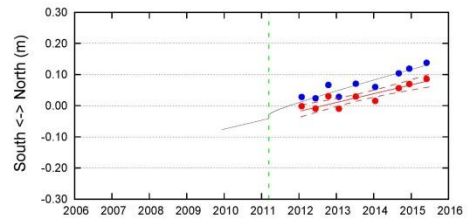
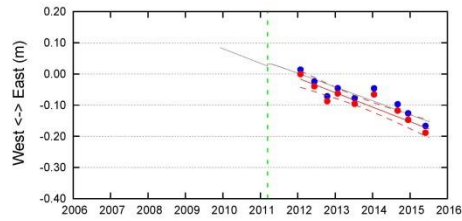
(8) MRT1



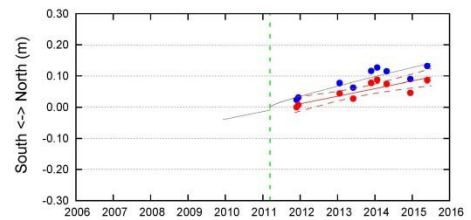
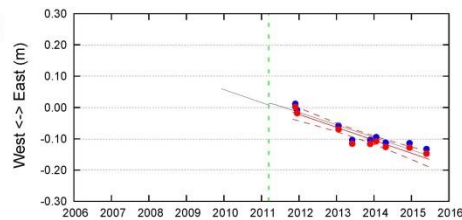
(9) MRT2



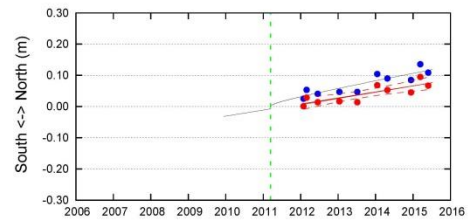
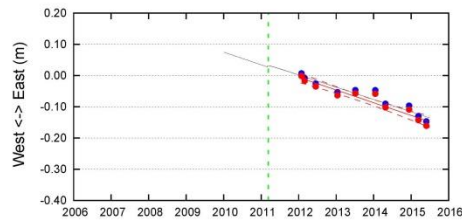
(10) TOS1

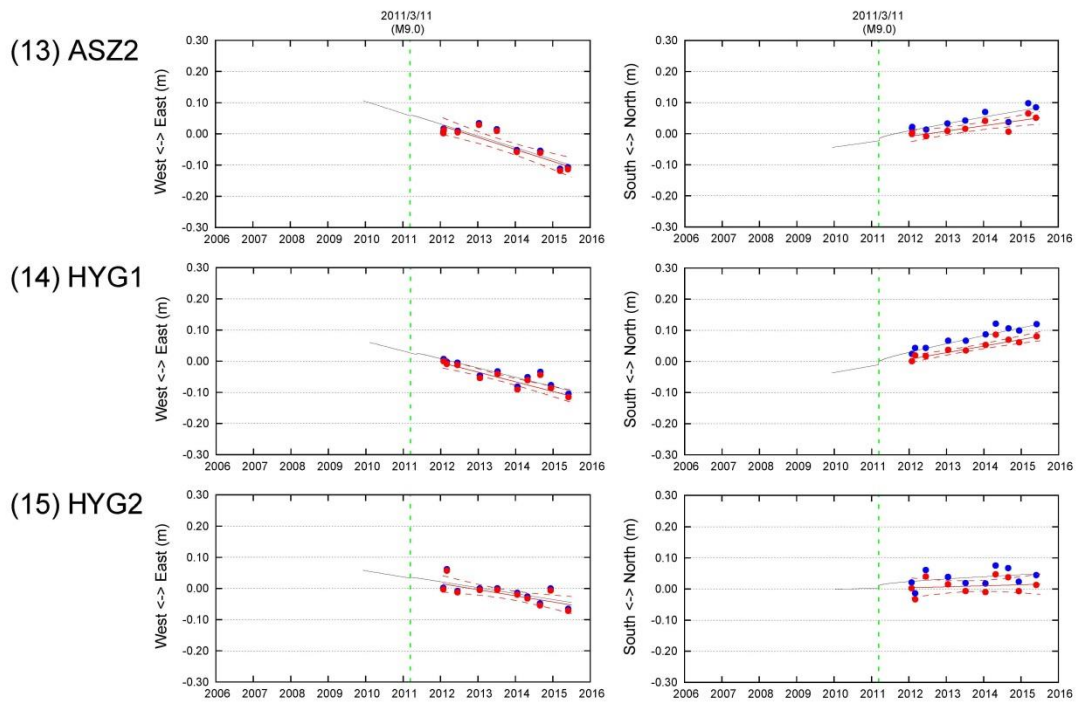


(11) TOS2



(12) ASZ1





**Extended Data Figures 2-4 | Time series in east-west (left column) and north-south (right column) displacements.** These data were obtained at the fifteen seafloor sites for the period after 2006. The position reference is the Amur plate. Blue circles indicate the raw observations before deductions of the coseismic and postseismic effects due to the 2011 Tohoku-oki earthquake. Red circles indicate the corrected final results. The linear trends and the 95% two-sided confidence intervals are shown with red solid and dashed lines, respectively. Black lines show the calculated coseismic and postseismic deformations following the Tohoku-oki earthquake<sup>18-19</sup>.

Site name	Position		Velocity (cm/year)			Standard deviation and Correlation (cm/year)		
	latitude	longitude	ABS (V)	east ( $V_e$ )	north ( $V_n$ )	$\sigma(e)$	$\sigma(n)$	$Corr(e, n)$
TOK1	34.08	138.14	5.0	-4.9	0.9	0.2	0.1	0.0
TOK2	33.88	137.61	4.9	-4.8	1.0	0.2	0.1	-0.1
TOK3	34.18	137.39	5.1	-5.1	0.8	0.4	0.5	-0.1
KUM1	33.67	137.00	3.6	-3.6	0.7	0.1	0.2	0.1
KUM2	33.43	136.67	4.3	-4.2	1.0	0.5	0.9	-0.5
KUM3	33.33	136.36	4.0	-3.9	1.0	0.2	0.2	-0.1
SIOW	33.16	135.57	4.7	-4.4	1.6	0.2	0.2	0.0
MRT1	33.35	134.94	3.4	-3.3	1.0	0.4	0.4	0.9
MRT2	32.87	134.81	3.9	-3.8	1.0	0.2	0.2	-0.1
TOS1	32.82	133.67	5.5	-4.7	2.8	0.6	0.4	-0.4
TOS2	32.43	134.03	4.8	-4.2	2.4	0.5	0.5	-0.4
ASZ1	32.37	133.22	4.5	-4.1	1.9	0.3	0.4	-0.2
ASZ2	31.93	133.58	4.2	-3.9	1.7	0.6	0.4	-0.5
HYG1	32.38	132.42	3.8	-3.1	2.1	0.4	0.3	-0.1
HYG2	31.97	132.49	2.0	-2.0	0.3	0.6	0.7	-0.6

**Table 1 | Velocity of each site with respect to the Amur plate with standard deviations and correlation.**

Extended Data Figs. 2, 3 and 4 show time series of the estimated horizontal coordinates of seafloor sites for each epoch relative to their locations in the first campaign. The reference frame is ITRF2005<sup>16</sup>. The positions are presented with respect to the stable part of the Amur plate, based on the MORVEL velocity model<sup>17</sup>. The position data of each epoch is summarized in Supplementary Table 1. Raw data from the six original sites involved coseismic deformation steps due to the Tohoku-oki earthquake. We removed these steps from raw data based on a coseismic source model established using onshore and seafloor geodetic data<sup>18</sup>. In addition, raw data from all sites involved postseismic deformations due to afterslip and viscoelastic relaxation following the Tohoku-oki earthquake. This nonlinear deformation was removed using the postseismic model calculated by means of a 3-D finite element method<sup>19</sup>.

The corrected data gave us seafloor velocity fields that reflect strain accumulation processes due to the Philippine Sea plate subduction under the upper Amur plate when all sites moved at stable displacement rates. Extended Data Figs. 2, 3 and 4 present linear trends fitted to the time series using a robust regression method (the  $M$  estimation method). Table 1 lists each velocity. The lines fitted to the EW and NS position time series in Extended Data Figs. 2, 3 and 4 represent the estimated linear station velocities and are shown with their 95% confidence intervals, which are used for the confidence ellipses shown in Fig. 1. The vertical velocities were not detected because they were smaller than detection limit (3 - 4 cm/year).

Long observation periods of the six original sites made the confidence ellipses small. These velocity fields are also compared with onshore GNSS data calculated for the stable period from March 2006 to December 2009 and the convergence rates of the Philippine Sea plate to the Amur plate in Fig. 1 calculated using the MORVEL model. These seafloor data are roughly consistent with the orientation of plate convergence and onshore velocities. Therefore, all offshore regions on the interplate boundary have positive SDRs.

These new data have great potential for advancing SDR distribution estimation<sup>20</sup>. Onshore data has no resolving power for offshore interplate boundaries, as described in the Methods section. Our seafloor data can show the offshore heterogeneity, though regions adjacent to the trench axis other than near TOK1 and ASZ2 cannot be resolved. The SDR distribution model established using these seafloor geodetic data is shown in Fig. 2a. The inversion strategy and detailed information are described in the Methods section, Supplementary Tables 2 and 3.



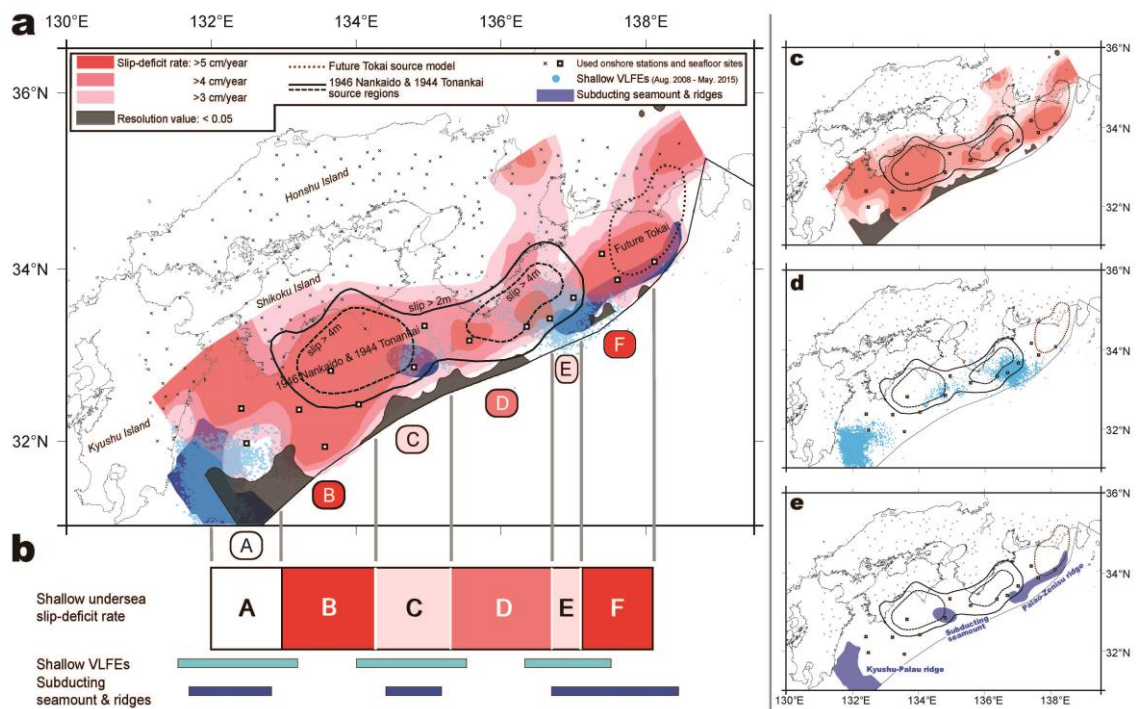


**Fig. 2 | Interplate SDR distribution indicated by the onshore and seafloor geodetic data.**

**a.** Contour map indicates the SDR distribution (SDR:  $> 3$  cm/year) obtained using the onshore and seafloor geodetic data. Light-blue dots and blue polygons indicate the shallow VLFES<sup>24</sup> and subducting seamount and ridges<sup>21-23</sup>, respectively. Dotted and solid polygons show the future Tokai source model<sup>5</sup> and the assumed large slip ( $> 2$  m) regions due to the 1946 Nankaido and 1944 Tonankai earthquakes<sup>2</sup>, respectively. Gray shadings indicate areas with resolution values lower than 0.05. **b.** A schematic illustration of the segmented source regions along the Nankai Trough. Upper figure shows a total conceptual illustration of the segmented high-SDR regions in the shallow side of the Nankai Trough. Dark colored region indicates a high-SDR. The regions of shallow VLFES and subducting seamounts are shown as bottom light-blue and blue bars, respectively. **c, d and e.** Separate figures of SDR distribution, shallow VLFES and subducting seamounts.

Along the Nankai Trough, subducting seamounts are located in three regions<sup>21-23</sup> where the very-low-frequency earthquakes (VLFs) were activated<sup>24</sup>. We mainly discuss the relation of the shallow SDR distribution with these seismological and geological features and the latest and predicted megathrust earthquake source regions from west to east. The deep part of this model is robustly similar to those in past studies using only onshore data<sup>8-10</sup>.

In region-A, an edge of the model region cannot be resolved enough. However, only our westernmost site HYG2 directly could catch a glimpse of the undersea SDR. The displacement rate at HYG2 was lower than those at adjacent sites (HYG1, ASZ1 and ASZ2) with certain confidence levels (95 %, 95 % and 90 % CL) according to the parallelism tests between each EW component. These data and our model suggest the VLF occurrence region extending to the east of the Kyushu-Palau ridge had a lower SDR than adjacent undersea regions. This spatial relation suggests that the subducting ridge not only activates shallow VLFs, but also forms the low-SDR region, that is, low-coupling condition.

In region-B, the deep high-SDR region corresponds with the latest megathrust earthquake source region. The region extends to the shallow side near the trench axis, which had no slip in the latest event. No conspicuous activity of the VLFs or subducting seamount was detected in this near-trench region. In this high-SDR region, patches of overshoot SDR (more than convergence rate: approximately 6.5 cm/year) exist as in past studies<sup>8-9</sup>. These are probably due to interseismic viscoelastic effects<sup>7</sup> or underestimation of the convergence rate.

This broad high-SDR region is segmented on the eastern region. This region-C is estimated to have a lower SDR than neighboring regions-B and D. Additionally, the VLF activity and the subducting seamount are located together, as in region-A. This spatial correspondence is additional evidence that the three phenomena have a physical correlation.

In region-D, where the Kii Peninsula protrudes to the south, the obtained SDR distribution corresponds with the latest earthquake source regions. The high-SDR region-F also corresponds with the future Tokai source model<sup>5</sup>. However, it reaches to the southwest region, which had no slip in the 1944 Tonankai earthquake and was not indicated as a future Tokai source model. These regions are partitioned by low-SDR region-E.

Below the shallow seafloor from regions-D to F, the Paleo-Zenisu ridge is subducting in the region nearest to the trench axis. On the other hand, intensive VLF activity is located in the gap region-E. Therefore, the low-SDR region-E has correlation

with the VLFE activity rather than the subducting ridge, though the resolving power is insufficient in the shallower south region as compared to our seafloor sites.

Observation studies<sup>25-26</sup> in the subduction zone worldwide had inferred the relation of the low-SDR condition with the subducting areas in front of topographic features, including seamounts. VLFE activity was also predicted to be related with the low-SDR condition<sup>27</sup>. In the Nankai Trough, indirect seismological evidence inferred the physical relation of the low-SDR condition with ridges and VLFES in recent seafloor research studies<sup>23,28</sup>, probably due to elevated pore-fluid pressure and a complicated fracture network. Three low-SDR regions-A, C and E discovered by our observation were the first direct evidences suggesting that subducting seamounts generate VLFE activity, which has low-SDR condition. It also suggests a possibility that VLFES are activated in the low-SDR region in front of subducting seamounts worldwide.

Fig. 2b shows a conceptual illustration of the segmented source regions discovered by our observation. This ‘shallow’ segmentation is inconsistent with the well-known ‘deep’ segmentation<sup>2</sup> of the Nankai Trough source region. Because the shallow high-SDR patches control the scale of tsunamis from megathrust ruptures, they are important for the assessment and early warning of the tsunami disaster. For example, the Tohoku-oki earthquake had a large amount of very shallow slip<sup>29</sup>, which led to a devastating tsunami. The high-SDR regions-B and F are located on the outer shallow regions of the most recent and anticipated earthquake source regions and have no historical earthquake record since the 1854 Ansei earthquakes<sup>2</sup>. These shallow regions have accumulated slip-deficit at least since 1854 and have the potential to drive shallow rupture and tsunami.

The low SDRs are indicated in regions-A, C and E, which segment the high-SDR (megathrust earthquake source) regions. For example, the 1944 Tonankai earthquake occurred on region-D and stopped at region-E in front of region-F<sup>1,3-4</sup>. However, when a rupture breaks through a segment boundary, a larger event is possible. The 1946 Nankaido earthquake progressed from region-D through region-C and finally reached the deep side of region-B<sup>1,3-4</sup>. In this way, the low-SDR regions control megathrust earthquake scenarios.

Our observation results and SDR distribution model reflect crustal deformation over only the last several years. We plan to perform continuous observations over decades to investigate the stability of interplate SDR distributions. We can also determine whether decadal changes in crustal deformation like those observed in eastern Japan<sup>29</sup> occur in this subduction zone.

## References

- (01) Kanamori, H. Tectonic implications of the 1944 Tonankai and the 1946 Nankaido earthquakes, Japan. *Phys.Earth Planet. Inter.* **5**, 129–139 (1972).
- (02) Ando, M. Source mechanism and tectonic significance of historical earthquakes along the Nankai Trough, Japan. *Tectonophysics* **27**, 119–140, doi:10.1016/0040-1951(75)90102-X (1975).
- (03) Sagiya, T. & Thatcher, W. Coseismic slip resolution along a plate boundary megathrust: The Nankai Trough, southwest Japan. *J. Geophys. Res.* **104**, B1, 1111–1129, doi:10.1029/98JB02644 (1999).
- (04) Baba, T. & Cummins, P. R. Contiguous rupture areas of two Nankai Trough earthquakes revealed by high-resolution tsunami waveform inversion. *Geophys. Res. Lett.* **32**, L083005, doi:10.1029/2004GL022320 (2005).
- (05) Central Disaster Management Council of the Japanese Government (2015) <http://www.bousai.go.jp/jishin/nankai/index.html> (in Japanese).
- (06) Moreno, M., Rosenau, M. & Oncken, O. 2010 Maule earthquake slip correlates with pre-seismic locking of Andean subduction zone. *Nature* **467**, 198–202, doi:10.1038/nature09349 (2010).
- (07) Wang, K., Hu, Y. & He, J. Deformation cycles of subduction earthquakes in a viscoelastic Earth. *Nature* **484**, 327–332, doi:10.1038/nature11032 (2012).
- (08) Ito, T. & Hashimoto, M., Spatiotemporal distribution of interplate coupling in southwest Japan from inversion of geodetic data. *J. Geophys. Res.* **109**, B02315, doi:10.1029/2002JB002358 (2004).
- (09) Hok, S., Fukuyama, E. & Hashimoto, C. Dynamic rupture scenarios of anticipated Nankai-Tonankai earthquakes, southwest Japan, *J. Geophys. Res.* **116**, B12319, doi:10.1029/2011JB008492 (2011).
- (10) Yoshioka, S. & Matsuoka, Y. Interplate coupling along the Nankai Trough, southwest Japan, inferred from inversion analyses of GPS data: Effects of subducting plate geometry and spacing of hypothetical ocean-bottom GPS stations, *Tectonophysics* **600**, 165–174, doi:10.1016/j.tecto.2013.01.023 (2013).
- (11) Asada, A. & Yabuki, T. Centimeter-level positioning on the seafloor. *Proc. Jpn Acad. Ser. B* **77**, 7–12 (2001).
- (12) Tadokoro, K., *et al.* Interseismic seafloor crustal deformation immediately above the source region of anticipated megathrust earthquake along the Nankai Trough, Japan. *Geophys. Res. Lett.* **39**, L10306, doi:10.1029/2012GL051696 (2012).
- (13) Spiess, F. N. *et al.* Precise GPS/Acoustic positioning of seafloor reference points for tectonic studies. *Phys.Earth Planet. Inter.* **108**, 101–112 (1998).

- (14) Gagnon, K., Chadwell, C. D. & Norabuena, E. Measuring the onset of locking in the Peru-Chile trench with GPS and acoustic measurements. *Nature* **434**, 205–208, doi:10.1038/nature03412 (2005).
- (15) Yokota, Y. *et al.* Heterogeneous interplate coupling along the Nankai Trough, Japan, detected by GPS-acoustic seafloor geodetic observation. *Progress Earth Planet. Sci.* **2**, 10, doi:10.1186/s40645-015-0040-y (2015).
- (16) Altamimi, Z., Collilieux, X., Legrand, J., Garayt, B. & Boucher, C. ITRF2005: A new release of the International Terrestrial Reference Frame based on time series of station positions and Earth Orientation Parameters. *Geophys. J. Int.* **112**, B09401, doi:10.1029/2007JB004949 (2007).
- (17) DeMets, C., Gordon, R. G. & Argus, D. F. Geologically current plate motions. *Geophys. J. Int.* **181**, 1–80, doi:10.1111/j.1365-246X.2009.04491.x (2010).
- (18) Iinuma, T., *et al.* Coseismic slip distribution of the 2011 off the Pacific Coast of Tohoku Earthquake (M9.0) refined by means of seafloor geodetic data. *J. Geophys. Res.* **117**, B07409, doi:10.1029/2012JB009186 (2012).
- (19) Sun, T. & Wang, K. Viscoelastic relaxation following subduction earthquakes and its effects on afterslip determination. *J. Geophys. Res.* **120**, 1329–1344, doi:10.1002/2004JB011707 (2015).
- (20) Yabuki, T. & Matsu'ura, M. Geodetic data inversion using a Bayesian information criterion for spatial distribution of fault slip. *Geophys. J. Int.* **109**, 363–375 (1992).
- (21) Kodaira, S., Takahashi, N., Nakanishi, A., Miura, S. & Kaneda, Y. Subducted seamount imaged in the rupture zone of the 1946 Nankaido earthquake. *Science* **289**, 104–106, doi:10.1126/science.289.5476.104 (2000).
- (22) Park, J.-O., Moore, G. F., Tsuru, T., Kodaira, S. & Kaneda, Y. A subducted oceanic ridge influencing the Nankai megathrust earthquake rupture. *Earth Planet. Sci. Lett.* **217**, 77–84, doi:10.1029/S0012-821X(03)00553-3 (2003).
- (23) Yamamoto, Y. *et al.* Imaging of the subducted Kyushu-Palau Ridge in the Hyuga-nada region, western Nankai Trough subduction zone. *Tectonophysics* **589**, 90–102, doi:10.1016/j.tecto.2012.12.028 (2013).
- (24) National Research Institute for Earth Science and Disaster Prevention, Activity of very-low-frequency earthquakes in and around Japan (November, 2014 – May, 2015) (in Japanese). *Report of the Coordinating Committee for Earthquake Prediction, Japan*, **94**, 5-7 (2015).
- (25) Chlieh, M., Avouac, J. P., Sieh, K., Natawidjaja, D., H. & Galetzka, J. Heterogeneous coupling of the Sumatran megathrust constrained by geodetic and

- paleogeodetic measurements. *J. Geophys. Res.* **113**, B05305, doi:10.1029/2007JB004981 (2008).
- (26) Perfettini, H., *et al.* Seismic and aseismic slip on the Central Peru megathrust. *Nature* **465**, 78–81, doi:10.1038/nature09062 (2010).
- (27) Hirose, H. *et al.* Slow earthquakes linked along dip in the Nankai subduction zone. *Science* **330**, 1502, doi:10.1126/science.1197102 (2010).
- (28) Yamashita, Y., *et al.* Migrating tremor off southern Kyushu as evidence for slow slip of a shallow subduction interface. *Science* **348**, 676–679, doi:10.1126/science.aaa4242 (2015).
- (29) Ozawa, S. *et al.* Preceding, coseismic, and postseismic slips of the 2011 Tohoku earthquake, Japan. *J. Geophys. Res.* **117**, B07404, doi:10.1029/2011JB009120 (2012).
- (30) Colombo, O. L. Long range kinematic GPS, in *GPS for Geodesy, 2nd Edition*, Kleusberg, A. & Teunissen, P., Editors. Springer-Verlag (1998).

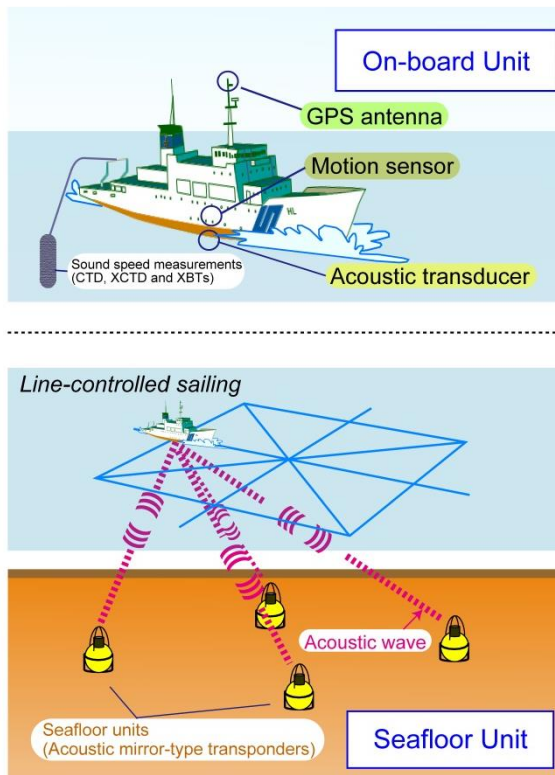
### **Acknowledgements**

We thank Professor R. Burgmann and Professor J.-P. Avouac for reviews and constructive comments that have helped improve this manuscript. We thank Dr. O. L. Colombo of the NASA Goddard Space Flight Center for providing us with the kinematic GPS software “IT” (Interferometric Translocation)<sup>30</sup> and the Geospatial Information Authority of Japan (GSI) for providing us with the high-rate GPS data for the kinematic GPS analysis and the daily coordinates of the sites on the GSI’s website. The coseismic and postseismic deformations of the 2011 Tohoku-oki earthquake were calculated by Dr. T. Iinuma and T. Sun, respectively. Comments from Professor K. Wang and Associate Professor A. Kato improved our manuscript. We thank T. Yabuki of the JHOD for providing us with the Bayesian inversion software. Additionally, many among the staff of the JHOD, including the crew of the S/Vs Takuyo, Shoyo, Meiyo and Kaiyo, have supported our observations and data processing. Some figures were produced using the GMT software by P. Wessel and W. H. F. Smith.

### **Author Contributions**

Y.Y. carried out the inversion analysis. T.I. designed the study and performed the statistical processing. Y.Y. and S.W. performed the resolution tests. Y.Y., T.I., S.W. and T.T. processed the GPS-A seafloor geodetic data. A.A. constructed the GPS-A system.

## Methods



**Extended Data Figure 1 | A schematic picture of our GPS-A seafloor geodetic observation system developed by ref. 11 and improved after ref. 35. This picture was modified from refs. 15, 34 and 37.**

### Seafloor geodetic observation

Since the radio wave scatters in the seawater, we measure the seafloor movements using the GPS observation above the sea and the acoustic ranging under the sea. This method is called as the GPS-A, which is a unique approach to monitor an absolute horizontal movement directly above the offshore interplate boundary. This technique was proposed in 1980s<sup>31</sup> and established after 1990s<sup>11,13-14</sup>. However, since their observation precision was lower than the present method, they achieved a robust observation result and needed an uneconomical very-long observation period. After 2000, the JHOD have been developing high-precise and sustainable observation techniques and provided valuable data for geodesy and seismology, e.g., the pre-, co- and post-seismic seafloor deformations of the 2011 Tohoku-oki earthquake<sup>32-34</sup>.

A schematic picture of our present seafloor geodetic observation system<sup>11,35-37</sup> is shown in Extended Data Fig. 1. This system consists of a seafloor unit with four

acoustic mirror-type transponders and an on-board unit with an undersea on-board acoustic transducer, a GPS antenna/receiver and a dynamic motion sensor. The on-board acoustic transducers were mounted at the stern of survey vessels for a drifting survey before 2007. After 2008, we provided a hull-mounted system to perform a line-controlled sailing survey<sup>37</sup> for stability and efficiency.

This system acquires three kinds of data. Kinematic GPS data are gathered to determine the absolute position of the survey vessel. Attitude data on the survey vessel are also obtained on board by a dynamic motion sensor to determine the coordinates of the on-board transducer relative to those of the GPS antenna. Distance data from the on-board transducer to the seafloor acoustic transponders are measured by acoustic ranging technique. The obtained roundtrip acoustic travel times are transformed to the ranges using sound speed profiles in seawater. These profiles are obtained using temperature and salinity profilers (conductivity temperature depth profiler (CTD), expendable conductivity temperature depth profiler (XCTD) and expendable bathythermographs (XBTs)) every several hours.

The consecutive absolute positions of the on-board transducer were determined by kinematic GPS analysis using IT software<sup>30</sup> and attitude data on the survey vessel. The position references are the onshore GEONET stations conducted by GSI<sup>38</sup>. The resultant position of the seafloor transponder was determined using a linearized inversion method based on a least squares formulation combining the absolute on-board transducer positions and the ranges to the seafloor acoustic transponders. This final analysis was constrained by the positional relationship of the grouped transponders for all epochs<sup>36</sup>. Here, this analysis cannot provide substantive information for positioning error of each epoch because we combine the independent observations to estimate all the positions.

To stabilize the estimates, we acquire acoustic ranging data of 3000 ~ 5000 shots for one observation at each site. We spent approximately 24 h performing an observation. Observation uncertainty of this technique is up to 2 - 3 centimeters in the horizontal component in each epoch. On the other hand, the vertical component has much uncertainty, because we observe the seafloor only from the upper region as similar as GNSS. A detection limit of the vertical velocity is 3 - 4 cm/year.

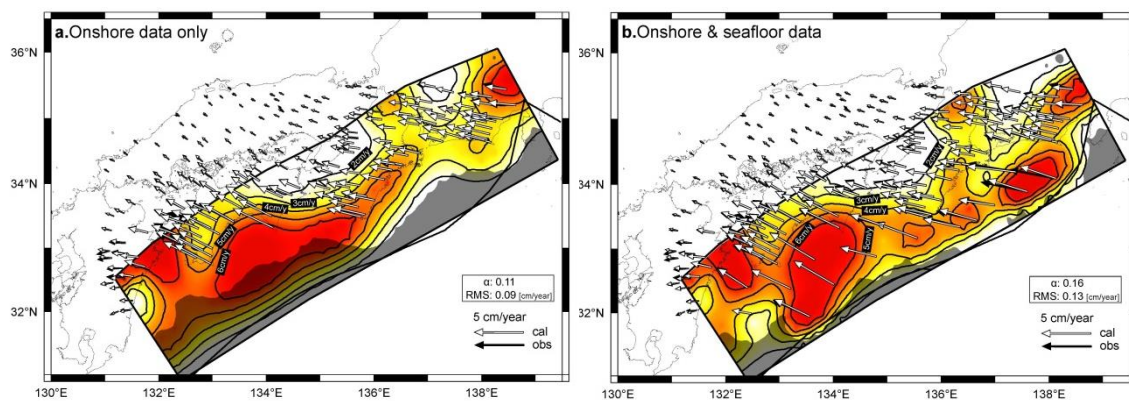
## **Data processing**

Raw seafloor geodetic observation data referred to the Amur Plate in MORVEL<sup>17</sup> are indicated as red circles before the Tohoku-oki earthquake and blue circles after this earthquake in Extended Data Figs. 2, 3 and 4. We deducted coseismic and non-linear postseismic effects due to the Tohoku-oki earthquake from these raw data. The

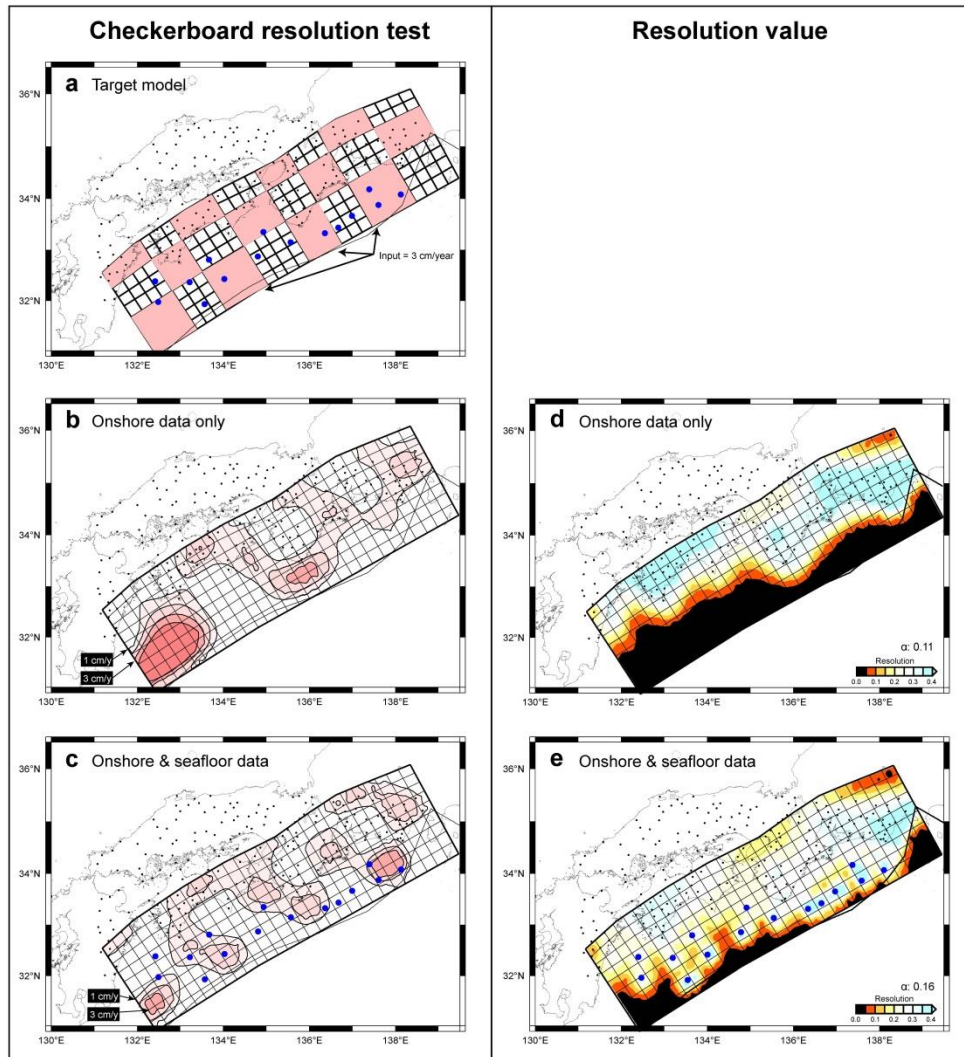


co-seismic effects were calculated based on the coseismic source model<sup>18</sup> established using many onshore stations of the GNSS network (GEONET, the University of Tohoku and others), seafloor geodetic data<sup>33,39</sup> and data of ocean bottom pressure gauges installed by the Earthquake Research Institute, the University of Tokyo. The postseismic effects were calculated based on the deformation model<sup>19</sup> established using this coseismic slip model and coordinated to match the GSI's onshore data and seafloor data (observed by the Tohoku University and us<sup>34</sup>) following the Tohoku-oki earthquake by means of the 3-D spherical-Earth finite element model. The prototype of this viscoelastic model was established in ref. 40 by including not only the mantle wedge and the oceanic mantle but also lithosphere-asthenosphere boundary based on the afterslip model developed by ref. 29. The revised model obtained in ref. 19 with regard to shallow afterslip was used in this study. These coseismic and postseismic effects were shown in Extended Data Figs. 2, 3 and 4. These are large in the eastern sites near the source region of the Tohoku-oki earthquake and very small in the western sites. The deducted data are indicated as red circles in Extended Data Figs. 2, 3 and 4. These final data and the raw data are listed in Supplementary Table 1.

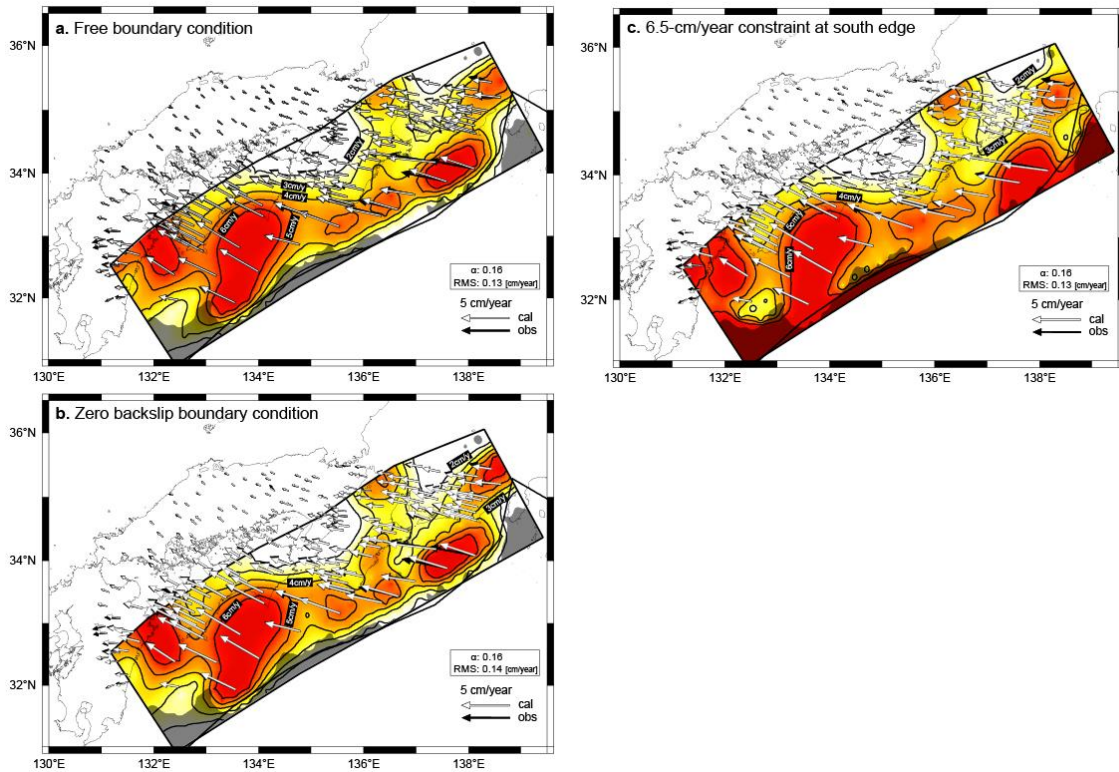
For estimations of the site velocities, we used a robust regression method (*M* estimation method) employing Turkey's biweight function. The negative influences of outliers mainly due to disturbances of an undersea sound speed structure were mitigated.



**Extended Data Figure 5 | Comparison of the calculated SDR distributions.** Resultant SDR distributions (SDR: > 2 cm/year) calculated (a) using only onshore data and (b) using onshore and seafloor data. Black and white vectors indicate the used data and calculated velocities, respectively. Gray shadings indicate areas with resolution values lower than 0.05 calculated in Extended Data Figs. 6d and 6e.



**Extended Data Figure 6 | Checker-board resolution tests and distributions of resolution values.** (Left) Results of checker-board resolution tests for the SDR inversions: **a.** Input checker-board like SDR distribution. The results of the cases **b.** using only onshore data and **c.** using both onshore and seafloor data. (Right) Resolution values as diagonal elements of the resolution matrix were also calculated for the cases **d.** using only onshore data and **e.** onshore and seafloor data, respectively.



**Extended Data Figure 7 | Examinations of boundary condition effects.** Estimated SDR distributions (SDR: > 2 cm/year) calculated with (a) free condition, (b) zero backslip condition at all the boundaries and (c) trench high-SDR condition. Gray shadings indicate areas with resolution values lower than 0.05 calculated in Extended Data Fig. 6e.

### Interplate SDR inversion method

We constructed the SDR distribution model by means of a geodetic inversion using the Yabuki and Matsu'ura method<sup>20</sup>. In this method, two prior constraints ( $\alpha$  and  $\sigma$ ) were included. We determined the best estimates of these hyperparameters by minimizing Akaike Bayesian Information Criterion (ABIC)<sup>41</sup> and obtained an optimal model. The SDR distribution model was coordinated to match our seafloor geodetic data and onshore GNSS data.

We set a fault model with approximately 800 km in the strike direction of  $237^\circ$  and approximately 300 km in the dip direction on the plate boundary. Our fault model was deployed simply on the interplate boundary model called as CAMP Standard Model<sup>42</sup>. We used a B-spline function as a basis function and calculated the SDR values by distributing subfaults on the plate boundary. Green's functions were calculated using

the formulation of ref. 20 considering a homogeneous elastic half-space. We deployed the broader model than the along-strike region around our seafloor sites. Thus, we also used the onshore GNSS data of GEONET around our fault model. These onshore data were calculated for the stable period from March 2006 to December 2009. In order to avoid biases in the inversion and keep smooth resolution of the SDR model, we sub-sampled the GEONET stations. The weight functions were set equally in all the onshore and offshore stations. Model boundary conditions are detailed in subsection: Model boundary condition effect.

The northern edge of our model would be affected by the block motions, because the block boundaries around the western Japan are located near the northern boundary of our model region. However, detailed investigation of block motions<sup>43</sup> showed that the maximum deformation rate of the block boundary (Median Tectonic Line) does not so much affect the undersea SDR distribution (less than 8 mm/year in the northernmost region of Shikoku Island and 3 mm/year in the eastern region). Intra-plate deformation has a negligible in this SDR model calculation. Although splay faults<sup>22,44-45</sup> have also an implication for the megathrust earthquakes and the tsunami generation, these smaller-scale fault geometries cannot be monitored and discussed by our present seafloor geodetic observation network.

Our resultant SDR distribution model is shown in Fig. 2 and Extended Data Fig. 5b. Hyperparameter values for the prior constraints ( $\alpha$  and  $\sigma$ ) were  $1.6 \times 10^{-1}$  and  $1.3 \times 10^{-1}$ . Our data improved the past model using only onshore data as shown in Extended Data Fig. 5a. The calculated SDR values for subfaults and the comparison between observed and calculated data are described in Supplementary Tables 2 and 3, respectively.

### **Resolution of the SDR inversion**

Checkerboard resolution tests were performed for examination of these data. We generated synthetic data for the checkerboard-like SDR distributions (Extended Data Fig. 6a) with errors (2-sigma: 0.3 cm/year and 1.5 cm/year for onshore and seafloor data). The synthetic data were inverted using the same parameters and settings as the SDR inversion. Extended Data Figs. 6b and 6c indicate the resultant distributions using only onshore data and using both onshore and seafloor data, respectively. An unsolved offshore region in Extended Data Fig. 6b was solved clearly in Extended Data Fig. 6c.

Extended Data Figs. 6d and 6e also show resolution values as diagonal elements of the resolution matrix calculated for the cases using only onshore data and onshore and seafloor data, respectively. The resolution matrix was represented as follows:

$$\mathbf{R} = (\mathbf{H}^T \mathbf{H} + \alpha^2 \mathbf{G}^T \mathbf{G})^{-1} \mathbf{H}^T \mathbf{H}$$

$\mathbf{H}$ : Static response function matrix

$\alpha$ : Hyperparameter of smoothness<sup>20</sup>

$\mathbf{G}$ : Spatial smoothness matrix<sup>20</sup>.

Undersea areas with low values shown in Extended Data Fig. 6d were improved by the seafloor data (Extended Data Fig. 6e), though the region adjacent to the trench axis cannot be resolved even with our seafloor network because there is no site.

Additionally, Green's functions for outer subfaults of interplate boundary (on the south of trench) were set to zero. These subfaults affect neighbor low-resolution subfaults through the spatial smoothing. By these reasons, a resolving power for the shallowest subfaults to the south of our seafloor sites was not sufficient as shown in Extended Data Fig. 6c.

### **Model boundary condition effect**

We examined the boundary condition of this inversion model. Each test was also calculated using the best hyperparameters determined by minimizing ABIC.

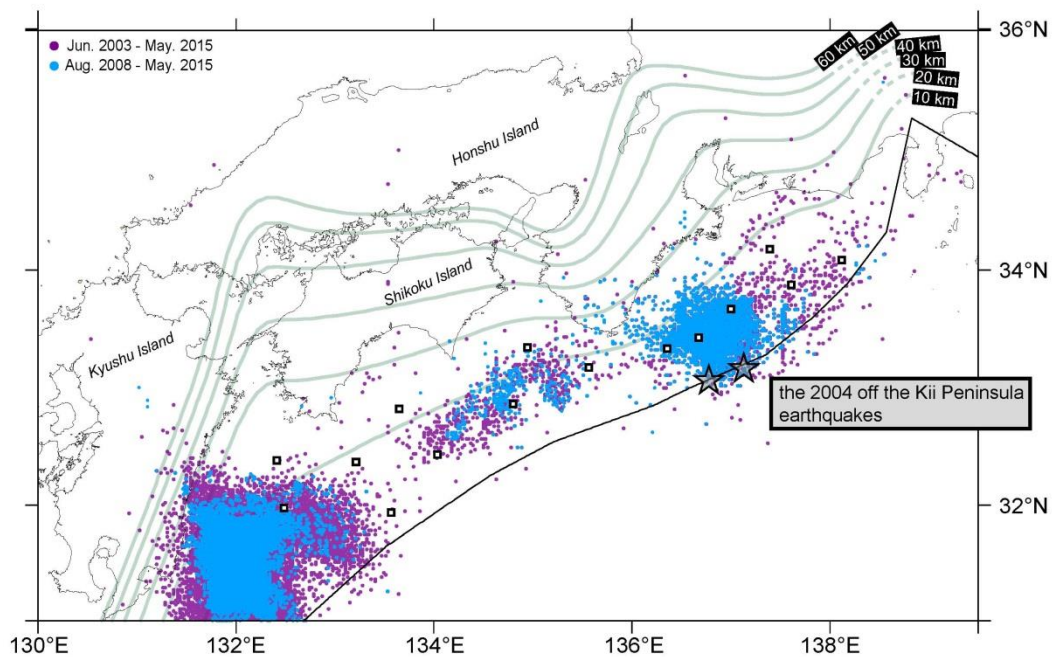
Our resultant SDR model was calculated with “zero backslip (full creeping)” condition at the trench side boundary and free condition at other model boundaries. Here, we calculated with free condition at all the boundaries, with zero backslip condition at all the boundaries and with 6.5 cm/year constraint at south edge (others: free condition), respectively, in order to examine the model boundary condition effect. Extended Data Figs. 7a, 7b and 7c showed the free condition, the zero backslip condition and the trench high-SDR condition results, respectively. These results suggest that the boundary condition did not control the main part of the undersea SDR calculation except for low-resolution shallow areas. There were small differences in the RMS of misfits between the observations and calculations in these cases.

### **VLFE distribution**

The VLFE distribution used in Figs. 2a and 2d was determined by automatic analysis<sup>24</sup> using the method of ref. 46. This approach separates VLFES and ordinary earthquakes automatically by comparing to NIED Hi-net catalogue. However, aftershocks following the M7 class event could not be fully differentiated. Then, we plotted the unordinary events (mainly VLFES) in the period of August 1, 2008 – May 10, 2015 without aftershocks of the 2004 off the Kii Peninsula earthquake. We also plotted all the events detected in the periods of June 1, 2003 – May 10, 2015 (Extended Data Fig. 8).

## Subducting seamounts

Reflection and refraction surveys were performed broadly along the Nankai Trough based on the past geomagnetic studies and seismic and bathymetric prior information. These surveys<sup>21-23</sup> detected three subducting seamounts (Figs. 2a and 2e) in front of the visible bathymetric features (Kyushu-Palau ridge, Kinan seamount chain and Zenisu ridge) shown in Fig. 1. The VLFEs were activated around these regions.



**Extended Data Figure 8 | Events determined using automatic VLFE detection analysis<sup>24</sup>.** Purple and light-blue dots denote events in the periods of June 1, 2003 – May 10, 2015 and August 1, 2008 – May 10, 2015, respectively. Gray stars indicate epicenters of the 2004 off the Kii Peninsula earthquakes. The depths of the plate boundary of CAMP model<sup>42</sup> are indicated by green lines.

## References

- (31) Spiess, F. N. Suboceanic geodetic measurements. *Geosci.Remote Sensing* **GE-23**, 4, 502–510 (1985).
- (32) Sato, M. *et al.* Interplate coupling off northeastern Japan before the 2011 Tohoku-oki earthquake, inferred from seafloor geodetic data. *J. Geophys. Res.* **118**, 1–10, doi:10.1002/jgrb.50275 (2013).
- (33) Sato, M. *et al.* Displacement above the hypocenter of the 2011 Tohoku-oki earthquake. *Science* **332**, 1395, doi:10.1126/science.1207401 (2011).
- (34) Watanabe, S. *et al.* Evidence of viscoelastic deformation following the 2011 Tohoku-oki earthquake revealed from seafloor geodetic observation. *Geophys. Res. Lett.* **41**, 5789–5796, doi:10.1002/2014GL061134 (2014).
- (35) Fujita, M. *et al.* GPS/acoustic seafloor geodetic observation: method of data analysis and its application. *Earth Planet. Space* **58**, 265–275, doi:10.1007/s00190-013-0649-9 (2006).
- (36) Matsumoto, Y., Fujita, M. & Ishikawa, T. Development of multi-epoch method for determining seafloor station position (in Japanese, Abstract in English). *Report of Hydrographic and Oceanographic Researches* **26**, 16–22 (2008).
- (37) Sato, M. *et al.* Improvement of GPS/acoustic seafloor positioning precision through controlling the ship's track line. *J. Geod.* **87**, 825–842, doi:10.1007/s00190-013-0649-9 (2013).
- (38) Sagiya, T., Miyazaki, S. & Tada, T. Continuous GPS array and present-day crustal deformation of Japan. *Pure Appl. Geophys.* **157**, 2303–2322, doi:10.1007/PL00022507 (2000).
- (39) Kido, M., Osada, Y., Fujimoto, H., Hino, R. & Ito, Y. Trench-normal variation in observed seafloor displacements associated with the 2011 Tohoku-Oki earthquake, *Geophys. Res. Lett.* **38**, L24303, doi:10.1029/2011GL050057 (2011).
- (40) Sun, T. *et al.* Prevalence of viscoelastic relaxation after the 2011 Tohoku-oki earthquake. *Nature* **514**, 84–87, doi:10.1038/nature13778 (2014).
- (41) Akaike, H. Likelihood and the Bayes procedure, in *Bayesian Statistics*, 143-166, Bernardo, J.M., DeGroot, M.H., Lindley, D.V. & Smith, A.F.M., Editors. University Press, Valencia (1980).
- (42) Hashimoto, C., Fukui, K. & Matsu'ura, M. 3-D modelling of plate interfaces and numerical simulation of long-term crustal deformation in and around Japan. *Pure Appl. Geophys.* **161**, 2053–2068 (2004).

- (43) Loveless, J. P. & Meade, B. J. Geodetic imaging of plate motions, slip rates, and partitioning of deformation in Japan. *J. Geophys. Res.* **115**, B02410, doi:10.1029/2008JB006248 (2010).
- (44) Park, J.-O., Tsuru, T., Kodaira, S., Cummins, P. R. & Kaneda, Y. Splay fault branching along the Nankai subduction zone, *Science* **297**, 1557–1560, doi:10.1126/science.1074111 (2002).
- (45) Moore, G. *et al.* Three-dimensional splay fault geometry and implications for Tsunami generation. *Science* **318**, 1128–1131, doi:10.1126/science.1147195 (2007).
- (46) Asano, Y., Obara, K. & Ito, Y. Spatiotemporal distribution of very-low frequency earthquakes in Tokachi-oki near the junction of the Kuril and Japan trenches revealed by using array signal processing. *Earth Planet. Space* **60**, 871–875, doi:10.1186/BF03352839 (2008).



## Supplementary Table legends

**Supplementary Table 1 | Estimated relative site positions.** The reference frame is ITRF2005. Eastward and Northward components indicate the data corrected the coseismic and postseismic effects due to the Tohoku-oki earthquake.  $East_{raw}$  and  $North_{raw}$  components are raw data after March 2011.

TOK1				
Epoch (year)	Eastward (m)	Northward (m)	$East_{raw}$ (m)	$North_{raw}$ (m)
2006.63	0	0		
2007.29	0.0313	-0.0173		
2008.54	0.0011	-0.0051		
2009.34	-0.026	0.01		
2009.55	0.0001	-0.0035		
2009.63	-0.007	-0.0094		
2010.6	-0.0818	-0.0221		
2010.95	-0.0409	-0.0016		
2011.07	-0.068	-0.0099		
2011.44	-0.0594	-0.0128	0.0024	0.0156
2011.94	-0.0715	-0.0285	-0.0005	0.0133
2012.42	-0.0517	-0.0443	0.0232	0.0069
2012.71	-0.0689	-0.0368	0.0077	0.0194
2013.09	-0.1327	-0.0213	-0.0539	0.0408
2013.4	-0.1482	-0.0461	-0.0674	0.0205
2013.5	-0.1252	-0.0094	-0.0437	0.0585
2013.88	-0.1395	-0.0256	-0.0556	0.047
2014.69	-0.1585	-0.1137	-0.0696	-0.0335
2015.21	-0.1733	-0.0263	-0.0813	0.0581

TOK2				
Epoch (year)	Eastward (m)	Northward (m)	$East_{raw}$ (m)	$North_{raw}$ (m)
2006.85	0	0		
2007.64	0.0008	0.0069		
2008.03	-0.0788	-0.0163		

2008.53	-0.0648	-0.002		
2008.53	-0.0828	-0.0132		
2009.1	-0.0999	-0.0222		
2009.55	-0.109	-0.0422		
2010.06	-0.1268	0.0106		
2010.6	-0.1071	-0.0271		
2010.96	-0.1207	-0.0099		
2011.07	-0.1272	0.001		
2011.44	-0.1839	-0.005	-0.1342	0.0233
2011.94	-0.1852	0.0003	-0.1279	0.0415
2012.77	-0.2016	-0.0223	-0.139	0.0337
2013.41	-0.1939	-0.0236	-0.1276	0.0414
2013.88	-0.2347	-0.0106	-0.1656	0.0602
2014.07	-0.2016	-0.0227	-0.1315	0.0502
2014.3	-0.2033	-0.0272	-0.1319	0.0478
2015.2	-0.2277	-0.0401	-0.1514	0.0425

---



---

TOK3

---



---

Epoch (year)	Eastward (m)	Northward (m)	East <sub>raw</sub> (m)	North <sub>raw</sub> (m)
2012.1	0	0	0	0
2012.15	-0.026	-0.0179	-0.0254	-0.0166
2012.42	-0.02	0.0206	-0.0166	0.0276
2013.08	0.0019	-0.0245	0.0109	-0.0056
2013.44	-0.0293	-0.0047	-0.0172	0.0199
2013.91	-0.0494	-0.0218	-0.0332	0.0094
2014.29	-0.0653	0.005	-0.0459	0.0408
2015.17	-0.0951	-0.0165	-0.0689	0.0279

---



---

KUM1

---



---

Epoch (year)	Eastward (m)	Northward (m)	East <sub>raw</sub> (m)	North <sub>raw</sub> (m)
2007.64	0	0		
2008.73	0.0246	0.0184		
2009.34	0.0216	0.0203		
2009.55	0.019	0.0011		

2009.83	0.0313	-0.0108		
2010.04	0.0623	-0.0227		
2010.6	0.0221	0.0253		
2011.06	0.0113	0.0094		
2011.44	0.022	0.0115	0.0607	0.0388
2012.77	-0.0223	0.0021	0.027	0.0546
2013.41	-0.0219	-0.0204	0.0305	0.0404
2013.51	-0.0139	-0.0148	0.0391	0.0472
2014.07	-0.047	-0.0194	0.0088	0.0486
2014.69	-0.0417	-0.0037	0.017	0.0696
2015.2	-0.0425	-0.0642	0.0186	0.0131

---



---

KUM2

---



---

Epoch (year)	Eastward (m)	Northward (m)	East <sub>raw</sub> (m)	North <sub>raw</sub> (m)
2012.09	0	0	0	0
2012.43	-0.0027	-0.0327	-0.0012	-0.0276
2013.07	-0.0336	0.016	-0.0295	0.0295
2013.43	-0.0112	-0.0186	-0.0056	-0.0011
2013.89	-0.0238	-0.0657	-0.0163	-0.0435
2014.3	-0.0567	-0.0174	-0.0475	0.0084
2014.98	-0.0458	-0.0114	-0.034	0.0194

---



---

KUM3

---



---

Epoch (year)	Eastward (m)	Northward (m)	East <sub>raw</sub> (m)	North <sub>raw</sub> (m)
2006.41	0	0		
2007.34	0.0535	0.021		
2007.66	0.0097	0.0294		
2008.71	0.0507	0.0434		
2009.11	0.0416	0.0304		
2009.33	0.0117	0.066		
2009.55	0.0322	0.0303		
2010.06	0.0089	0.0092		
2010.6	0.0097	0.0137		
2011.06	0.0159	0.018		

2011.44	-0.0131	0.0133	0.014	0.0381
2011.9	-0.0057	0.0277	0.0253	0.0619
2011.95	-0.0255	0.0158	0.0057	0.0508
2012.8	-0.0233	-0.0203	0.0113	0.0264
2013.43	-0.0502	-0.03	-0.0132	0.0238
2013.89	-0.0513	0.0453	-0.0125	0.1035
2014.69	-0.0415	0.0006	0.0002	0.065
2015.18	-0.0777	0.0414	-0.0343	0.1093

---



---

SIOW

---



---

Epoch (year)	Eastward (m)	Northward (m)	East <sub>raw</sub> (m)	North <sub>raw</sub> (m)
2006.69	0	0		
2007.65	-0.0583	-0.044		
2008.04	0.0016	-0.0475		
2008.71	-0.0133	-0.0594		
2009.32	-0.0805	-0.031		
2009.55	-0.05	-0.04		
2010.05	-0.0604	-0.0253		
2010.6	-0.0728	-0.0092		
2011.06	-0.1209	-0.0232		
2011.44	-0.0768	-0.0094	-0.055	0.0152
2011.95	-0.0848	-0.0125	-0.0596	0.0214
2012.78	-0.0811	-0.0212	-0.0529	0.0233
2013.06	-0.1283	-0.0246	-0.0991	0.0229
2013.43	-0.104	-0.0208	-0.0735	0.0303
2013.89	-0.1684	-0.0163	-0.1363	0.0389
2014.68	-0.1412	0.0097	-0.1065	0.0707
2014.97	-0.1927	-0.0198	-0.1571	0.0432

---



---

MRT1

---



---

Epoch (year)	Eastward (m)	Northward (m)	East <sub>raw</sub> (m)	North <sub>raw</sub> (m)
2012.09	0	0	0	0
2012.16	0.0114	0.028	0.0117	0.0289
2012.44	-0.0216	-0.0093	-0.0201	-0.0048

2012.78	-0.0058	0.0049	-0.0029	0.0133
2013.43	-0.0253	-0.0073	-0.0196	0.0077
2013.9	-0.0505	-0.0241	-0.0428	-0.0049
2014.67	-0.0221	-0.008	-0.0114	0.017
2014.97	-0.0251	0.0033	-0.0134	0.0304

---



---

MRT2

---



---

Epoch (year)	Eastward (m)	Northward (m)	East <sub>raw</sub> (m)	North <sub>raw</sub> (m)
2006.67	0	0		
2007.35	0.0084	-0.043		
2008.71	0.0184	-0.0375		
2009.11	-0.0125	-0.0438		
2009.33	0.0071	-0.0116		
2009.56	0.0021	-0.0562		
2010.05	0.0252	-0.0557		
2010.6	-0.0253	-0.043		
2010.96	-0.0364	-0.0619		
2011.44	-0.0056	-0.0977	0.0098	-0.0756
2011.95	-0.0271	-0.0627	-0.0093	-0.0326
2012.78	-0.0568	-0.0637	-0.0368	-0.0248
2013.06	-0.0538	-0.0593	-0.0331	-0.0179
2013.42	-0.0256	-0.0456	-0.0039	-0.0012
2013.89	-0.0732	-0.0693	-0.0502	-0.0213
2014.3	-0.0767	-0.0774	-0.0527	-0.0267
2014.67	-0.0267	-0.063	-0.0019	-0.0101
2014.95	-0.0731	-0.0122	-0.0476	0.0423
2015.18	-0.1112	-0.032	-0.0852	0.0238
2015.43	-0.1069	-0.0431	-0.0804	0.0141

---



---

TOS1

---



---

Epoch (year)	Eastward (m)	Northward (m)	East <sub>raw</sub> (m)	North <sub>raw</sub> (m)
2012.07	0	0	0	0
2012.44	-0.03	-0.0124	-0.0291	-0.0089
2012.79	-0.0696	0.0233	-0.0679	0.0296

2013.07	-0.0378	-0.0204	-0.0354	-0.012
2013.52	-0.0602	0.0129	-0.0567	0.0245
2014.04	-0.0174	-0.0074	-0.0127	0.0075
2014.67	-0.054	0.0254	-0.0481	0.0437
2014.95	-0.0769	0.0353	-0.0704	0.0551
2015.41	-0.1072	0.046	-0.0999	0.0682

---

---

TOS2

---

---

Epoch (year)	Eastward (m)	Northward (m)	East <sub>raw</sub> (m)	North <sub>raw</sub> (m)
2011.9	0	0	0	0
2011.95	-0.0188	0.0066	-0.0187	0.0071
2013.06	-0.0438	0.03	-0.0421	0.0392
2013.42	-0.0809	0.0087	-0.0787	0.0202
2013.9	-0.07	0.0527	-0.067	0.067
2014.06	-0.0576	0.0605	-0.0544	0.0757
2014.31	-0.0696	0.0443	-0.066	0.0608
2014.95	-0.0564	0.0083	-0.0521	0.0277
2015.4	-0.0648	0.0427	-0.0599	0.0642

---

---

ASZ1

---

---

Epoch (year)	Eastward (m)	Northward (m)	East <sub>raw</sub> (m)	North <sub>raw</sub> (m)
2012.08	0	0	0	0
2012.16	-0.0133	0.0266	-0.0132	0.0272
2012.46	-0.0243	0.0081	-0.0238	0.0109
2013.04	-0.0383	0.0035	-0.037	0.01
2013.51	-0.0207	-0.0052	-0.0188	-0.004
2014.04	-0.0088	0.043	-0.0061	0.0549
2014.32	-0.0461	0.024	-0.0431	0.0371
2014.95	-0.0375	0.0087	-0.0338	0.0245
2015.2	-0.0652	0.0552	-0.0613	0.072
2015.41	-0.0769	0.0246	-0.0728	0.0423

---

---

ASZ2

---

---

Epoch (year)	Eastward (m)	Northward (m)	East <sub>raw</sub> (m)	North <sub>raw</sub> (m)
2012.08	0	0	0	0
2012.09	0.0102	0.0038	0.0102	0.0039
2012.46	0.0124	-0.0117	0.0126	-0.0094
2013.03	0.0502	-0.002	0.0507	0.0033
2013.51	0.0422	-0.0009	0.0431	0.0066
2014.04	-0.0121	0.0178	-0.0108	0.0275
2014.67	0.0005	-0.0247	0.0021	-0.0127
2015.2	-0.0444	0.0276	-0.0426	0.0414
2015.4	-0.0343	0.0113	-0.0324	0.0258

---



---

HYG1

---



---

Epoch (year)	Eastward (m)	Northward (m)	East <sub>raw</sub> (m)	North <sub>raw</sub> (m)
2012.08	0	0	0	0
2012.16	-0.0066	0.0177	-0.0065	0.0183
2012.45	-0.0032	0.0123	-0.0027	0.0148
2013.04	-0.0304	0.0245	-0.0292	0.0305
2013.52	-0.0061	0.0165	-0.0043	0.0249
2014.05	-0.0427	0.0278	-0.0403	0.0387
2014.32	-0.0061	0.0575	-0.0034	0.0695
2014.66	0.0191	0.0368	0.0221	0.0502
2014.94	-0.0168	0.0251	-0.0136	0.0396
2015.41	-0.0339	0.0383	-0.0303	0.0546

---



---

HYG2

---



---

Epoch (year)	Eastward (m)	Northward (m)	East <sub>raw</sub> (m)	North <sub>raw</sub> (m)
2012.07	0	0	0	0
2012.17	0.0622	-0.0368	0.0622	-0.0362
2012.45	-0.0006	0.0333	-0.0004	0.0354
2013.05	0.0215	0.0008	0.0221	0.0057
2013.52	0.0333	-0.0266	0.0343	-0.0197
2014.05	0.0314	-0.0366	0.0328	-0.0277
2014.32	0.0258	0.0168	0.0274	0.0266

2014.66	0.0118	0.0035	0.0135	0.0144
2014.94	0.0665	-0.0446	0.0684	-0.0328
2015.41	0.0127	-0.0308	0.0148	-0.0176

---

---



**Supplementary Table 2 | Position and calculated SDR value of each subfault in the inversion analysis.** First and second columns show location (longitude and latitude) of each subfault. Third and fourth columns show angle (from the east to the counterclockwise direction) and absolute SDR value (m/year) calculated for each subfault in the inversion.

LON(E)	LAT(N)	ANGLE	ABSOLUTE VALUE[m/year]
132.511	31.041	-143.373	0.0077
132.743	31.169	-133.469	0.0077
132.976	31.296	-135.328	0.0083
133.21	31.422	-150.873	0.0121
133.445	31.549	-161.94	0.0189
133.68	31.675	-168.515	0.0233
133.916	31.8	-175.832	0.022
134.153	31.925	170.747	0.0162
134.39	32.049	153.338	0.0117
134.628	32.173	145.007	0.0097
134.866	32.297	150.987	0.0089
135.106	32.42	165.316	0.0087
135.346	32.542	171.046	0.0099
135.586	32.664	162.653	0.0131
135.828	32.785	160.316	0.0153
136.07	32.906	160.591	0.0153
136.313	33.027	157.388	0.0154
136.557	33.146	160.04	0.0182
136.801	33.266	164.781	0.0191
137.046	33.384	170.011	0.0143
137.292	33.503	179.921	0.0178
137.539	33.62	-176.997	0.0265
137.786	33.737	-177.636	0.0278
138.035	33.854	176.539	0.0256
138.284	33.97	169.738	0.0225
138.533	34.085	168.921	0.017
138.784	34.2	164.725	0.0084
139.035	34.314	90.647	0.0014
139.288	34.427	-3.338	0.0033

132.362	31.24	-145.816	0.0255
132.595	31.368	-135.005	0.0245
132.829	31.496	-135.665	0.025
133.063	31.623	-151.855	0.036
133.298	31.749	-163.251	0.0567
133.533	31.876	-170.083	0.0705
133.769	32.001	-177.902	0.0674
134.006	32.126	168.09	0.051
134.244	32.251	151.463	0.0383
134.482	32.375	144.659	0.0324
134.721	32.499	150.978	0.0298
134.961	32.622	165.319	0.0281
135.201	32.745	171.167	0.0311
135.443	32.866	161.839	0.0408
135.685	32.988	159.047	0.0474
135.927	33.108	159.828	0.047
136.171	33.229	157.805	0.0461
136.415	33.349	160.505	0.0543
136.66	33.468	164.631	0.0571
136.905	33.588	169.406	0.042
137.151	33.707	179.176	0.0518
137.398	33.825	-177.917	0.0774
137.646	33.942	-178.735	0.0816
137.894	34.059	175.611	0.0757
138.144	34.175	169.234	0.067
138.394	34.291	168.515	0.0508
138.645	34.406	164.35	0.0255
138.897	34.52	96.337	0.004
139.149	34.634	-8.721	0.0094
132.214	31.439	-153.706	0.04
132.447	31.567	-141.557	0.0327
132.681	31.695	-138.542	0.0266
132.915	31.822	-158.056	0.036
133.15	31.949	-170.29	0.0598
133.386	32.076	-177.761	0.078
133.622	32.202	172.861	0.0794

133.86	32.327	158.047	0.0679
134.098	32.452	145.644	0.0581
134.336	32.576	143.731	0.0517
134.576	32.7	150.75	0.0472
134.816	32.823	164.68	0.041
135.057	32.946	170.857	0.0404
135.299	33.068	158.148	0.0512
135.542	33.189	153.699	0.0591
135.785	33.309	156.285	0.0557
136.029	33.429	159.336	0.0492
136.274	33.549	162.093	0.0571
136.519	33.669	163.043	0.0607
136.764	33.79	165.244	0.0412
137.01	33.91	173.97	0.0471
137.257	34.029	176.406	0.0723
137.505	34.146	174.91	0.0782
137.754	34.263	170.37	0.0753
138.004	34.379	166.309	0.0687
138.255	34.496	166.463	0.0536
138.506	34.611	162.994	0.0286
138.758	34.726	135.172	0.0047
139.01	34.841	-42.067	0.0083
132.065	31.637	-166.816	0.0475
132.298	31.766	-163.192	0.0323
132.532	31.894	-174.867	0.0177
132.767	32.021	162.834	0.0238
133.002	32.149	162.798	0.0403
133.238	32.275	160.74	0.0568
133.475	32.401	154.144	0.0671
133.713	32.527	145.565	0.0698
133.952	32.652	142.409	0.068
134.191	32.776	145.242	0.064
134.43	32.9	150.023	0.0586
134.671	33.023	158.777	0.047
134.913	33.146	162.578	0.0396
135.156	33.267	148.687	0.047

135.4	33.387	143.108	0.0526
135.644	33.507	148.163	0.0448
135.889	33.627	163.769	0.0336
136.134	33.748	167.969	0.0395
136.379	33.869	161.226	0.0449
136.624	33.99	156.246	0.029
136.869	34.112	154.455	0.0247
137.116	34.232	155.292	0.0343
137.365	34.349	153.674	0.0389
137.615	34.465	155.544	0.0412
137.866	34.581	160.16	0.042
138.117	34.697	163.817	0.0386
138.368	34.814	162.392	0.0294
138.619	34.93	165.36	0.0186
138.871	35.047	-160.699	0.0152
131.916	31.835	179.363	0.0513
132.148	31.965	167.627	0.0404
132.383	32.093	142.174	0.0344
132.618	32.221	132.343	0.041
132.854	32.348	137.297	0.0452
133.091	32.474	142.562	0.0539
133.328	32.6	143.852	0.0654
133.566	32.726	144.357	0.0729
133.805	32.851	147.184	0.0753
134.045	32.975	149.871	0.0739
134.285	33.1	148.929	0.0686
134.526	33.223	148.905	0.0559
134.769	33.344	147.982	0.0456
135.014	33.464	141.284	0.0482
135.259	33.583	137.763	0.0485
135.504	33.703	144.268	0.0387
135.75	33.823	170.472	0.0309
135.995	33.944	175.116	0.0412
136.24	34.066	165.232	0.0507
136.484	34.188	160.814	0.041
136.729	34.312	156.037	0.0311

136.975	34.433	149.24	0.0284
137.225	34.55	145.077	0.028
137.477	34.664	152.655	0.0305
137.729	34.779	163.814	0.0369
137.981	34.895	168.361	0.0438
138.232	35.012	164.854	0.0475
138.484	35.129	162.993	0.0483
138.735	35.248	172.213	0.0476
131.769	32.028	173.113	0.0446
131.999	32.162	156.953	0.0492
132.233	32.292	141.669	0.0558
132.468	32.42	137.858	0.0604
132.704	32.547	142.42	0.0532
132.942	32.674	146.413	0.0522
133.18	32.799	146.988	0.0606
133.419	32.924	148.962	0.0699
133.659	33.049	151.73	0.0753
133.899	33.174	152.055	0.0752
134.139	33.298	147.88	0.0698
134.381	33.422	145.399	0.0579
134.625	33.542	147.418	0.0458
134.872	33.659	150.995	0.0407
135.12	33.776	152.511	0.0341
135.367	33.894	161.331	0.0244
135.613	34.014	-169.428	0.0221
135.858	34.135	-174.42	0.0322
136.103	34.258	170.717	0.0436
136.347	34.383	166.917	0.0435
136.589	34.51	164.585	0.038
136.834	34.634	158.084	0.0317
137.085	34.75	151.575	0.0257
137.339	34.863	158.435	0.0248
137.592	34.976	170.922	0.0318
137.847	35.089	173.824	0.0437
138.102	35.202	166.972	0.0555
138.355	35.318	161.692	0.0646

138.606	35.438	165.788	0.0675
131.63	32.209	-175.178	0.0288
131.853	32.354	160.225	0.0468
132.083	32.489	147.516	0.0674
132.318	32.619	145.41	0.0732
132.554	32.747	151.259	0.0572
132.793	32.873	154.85	0.0463
133.032	32.998	151.486	0.0492
133.272	33.122	151.081	0.0584
133.512	33.247	151.653	0.0643
133.752	33.372	150.062	0.0641
133.993	33.497	145.897	0.0594
134.236	33.62	146.064	0.0484
134.483	33.737	156.882	0.035
134.733	33.851	178.464	0.027
134.983	33.964	-163.278	0.0205
135.231	34.081	-141.558	0.0136
135.477	34.202	-115.701	0.0124
135.722	34.325	-141.512	0.0132
135.967	34.449	-174.858	0.0215
136.21	34.575	-179.236	0.0304
136.45	34.705	177.877	0.035
136.693	34.834	169.185	0.0331
136.946	34.948	161.35	0.0248
137.202	35.059	166.28	0.0183
137.457	35.17	-178.008	0.0202
137.716	35.279	-176.851	0.0305
137.975	35.386	170.653	0.0444
138.232	35.497	161.273	0.0574
138.484	35.615	162.266	0.0621
131.505	32.373	-125.698	0.0288
131.717	32.532	-177.212	0.039
131.939	32.679	154.713	0.066
132.169	32.815	146.718	0.0766
132.404	32.945	147.015	0.0571
132.643	33.071	146.757	0.0389

132.883	33.196	144.008	0.0365
133.124	33.32	146.72	0.0427
133.365	33.444	148.441	0.0454
133.606	33.569	146.811	0.0438
133.846	33.695	144.58	0.0417
134.09	33.818	148.035	0.0328
134.34	33.931	168.965	0.0194
134.596	34.038	-139.646	0.0138
134.85	34.147	-110.622	0.0122
135.1	34.263	-90.404	0.007
135.345	34.385	-42.584	0.0051
135.589	34.51	-59.877	0.0042
135.833	34.635	-130.869	0.0103
136.075	34.764	-145.393	0.0241
136.312	34.9	-156.112	0.0355
136.551	35.034	-171.422	0.039
136.806	35.146	178.998	0.0308
137.067	35.251	-176.881	0.0186
137.326	35.358	-152.055	0.0119
137.588	35.462	-144.708	0.0146
137.852	35.563	-171.142	0.0196
138.115	35.667	166.033	0.027
138.373	35.778	161.08	0.031
131.394	32.517	-108.03	0.0599
131.595	32.691	-139.019	0.0546
131.805	32.854	178.188	0.063
132.025	33.004	158.884	0.074
132.255	33.141	154.015	0.0601
132.493	33.269	153.311	0.0429
132.734	33.393	156.196	0.0364
132.977	33.515	164.363	0.0368
133.219	33.639	171.855	0.034
133.46	33.765	175.483	0.0285
133.699	33.892	173.862	0.0261
133.942	34.016	177.879	0.0202
134.199	34.122	-152.679	0.0109

134.463	34.218	-81.386	0.0095
134.723	34.32	-40.108	0.0062
134.976	34.433	74.93	0.0065
135.223	34.554	91.232	0.0125
135.466	34.68	113.644	0.0091
135.709	34.807	-157.56	0.0136
135.947	34.942	-141.394	0.0335
136.176	35.09	-144.929	0.0499
136.408	35.235	-161.078	0.0558
136.668	35.341	-171.413	0.0435
136.935	35.437	-162.489	0.0213
137.201	35.536	-75.845	0.01
137.47	35.631	-42.007	0.0195
137.742	35.721	-31.726	0.0193
138.014	35.812	-9.051	0.014
138.281	35.911	24.465	0.0116



**Supplementary Table 3 | Observed and calculated vectors of each site in the inversion analysis.** First and second columns show location (longitude and latitude) of each site. Third and fourth columns show angle (from the east to the counterclockwise direction) and absolute velocity value (m/year) observed in each site. Fifth and sixth columns show angle and absolute velocity value calculated for each site in the inversion.

LON(E)	LAT(N)	obs(ANG,	ABS[m/y])	calc(ANG,	ABS[m/y])
135.4	33.745	164.646	0.0279	163.81	0.028
136.338	34.65	174.75	0.0197	176.701	0.0186
131.798	33.24	166.176	0.0209	164.742	0.0205
133.682	33.938	149.24	0.0217	150.588	0.0215
132.458	34.894	144.851	0.0048	138.315	0.0052
136.165	35.096	175.447	0.0156	179.733	0.0159
134.395	34.219	151.181	0.0144	149.485	0.0144
132.195	34.371	140.015	0.0086	141.4	0.0073
135.77	33.484	165.501	0.0369	164.757	0.0368
135.761	35.488	175.315	0.0091	161.152	0.0082
138.118	34.68	166.015	0.03	165.542	0.0306
131.365	32.528	175.798	0.0186	179.689	0.0151
135.389	33.962	166.049	0.0246	166.933	0.0227
137.165	34.918	166.522	0.0244	167.154	0.0239
132.991	34.079	144.582	0.0144	140.846	0.0142
135.714	33.638	167.329	0.0311	166.102	0.0311
131.149	32.457	-168.614	0.0119	-173.386	0.0134
136.862	34.466	163.368	0.0245	163.604	0.0264
133.806	33.655	151.003	0.0298	151.854	0.0305
131.416	34.441	137.085	0.0051	146.598	0.0049
134.237	35.022	155.266	0.0059	150.109	0.0062
131.066	34.181	143.898	0.0051	150.477	0.0049
135.74	33.97	169.276	0.0234	172.397	0.023
137.352	34.787	165.712	0.0254	163.822	0.0255
133.193	35.313	144.613	0.0031	137.542	0.0044
138.179	34.634	164.994	0.0322	167.227	0.0327
131.384	33.079	177.419	0.0171	170.824	0.015
132.903	35.312	94.142	0.0029	137.115	0.0043
138.036	34.786	166.515	0.0275	165.135	0.0275

137.327	35.04	166.407	0.0226	168.292	0.023
135.877	35.138	173.902	0.0128	174.688	0.0127
131.531	32.557	174.548	0.0163	173.257	0.0163
133.901	34.327	143.218	0.0117	144.79	0.0119
135.595	33.748	166.927	0.0279	166.734	0.0276
135.671	34.99	169.514	0.0124	170.96	0.0127
137.291	34.649	165.953	0.0262	160.715	0.0269
133.962	34.984	154.705	0.0059	145.379	0.0059
134.662	34.866	157.786	0.0075	158.968	0.0079
136.549	34.286	174.342	0.0237	168.754	0.0251
132.487	33.612	153.855	0.0214	152.178	0.0209
132.885	34.211	140.213	0.0119	138.489	0.0114
131.132	32.845	-173.677	0.0148	173.544	0.0129
135.632	34.48	169.355	0.0178	171.891	0.0169
138.271	34.954	168.528	0.0263	168.393	0.0262
133.34	35.438	120.361	0.0028	137.931	0.0042
133.876	34.041	142.28	0.0191	148.874	0.0192
135.184	33.915	159.933	0.0244	164.447	0.0234
131.093	32.951	-165.676	0.014	171.308	0.0119
132.281	33.47	158.443	0.0218	156.772	0.0215
133.338	34.779	144.965	0.0065	137.579	0.0065
133.802	34.739	146.976	0.0064	142.471	0.0068
133	32.992	153.603	0.0396	153.261	0.0399
134.738	34.335	154.364	0.0132	154.884	0.0128
133.281	33.469	153.651	0.0332	152.392	0.0322
134.158	35.342	159.677	0.0049	145.167	0.0052
134.774	35.164	165.357	0.0066	154.198	0.0073
137.711	35.08	167.954	0.0229	170.041	0.0223
135.225	34.159	165.156	0.0198	163.53	0.0185
131.169	33.497	159.739	0.0093	158.743	0.0087
135.362	34.257	162.49	0.0186	166.136	0.0178
135.92	35.353	173.772	0.0107	171.64	0.0106
132.489	33.04	157.924	0.0317	153.1	0.0345
132.361	33.203	154.487	0.028	159.162	0.0293
137.086	35.24	169.114	0.0212	171.004	0.0203
133.565	35.171	147.06	0.004	139.784	0.005

134.239	35.268	159.529	0.0055	147.05	0.0055
135.691	34.779	174.374	0.0161	172.687	0.0148
134.628	33.928	157.505	0.0236	160.218	0.0219
134.976	35.092	160.802	0.0085	157.861	0.0083
134.101	33.498	154.277	0.0386	154.003	0.0378
132.744	33.306	156.395	0.0293	157.801	0.0306
134.051	35.177	159.96	0.0052	145.676	0.0054
138.206	35.322	173.441	0.0214	171.997	0.0233
138.275	35.201	168.883	0.0268	171.071	0.0271
137.944	35.318	167.393	0.0214	171.72	0.0199
133.09	33.417	153.419	0.0316	154.115	0.0318
134.821	35.317	161.679	0.0064	150.805	0.0068
133.048	33.885	149.047	0.0191	146.986	0.0192
135.069	34.273	153.992	0.0147	160.538	0.0156
132.358	33.911	145.689	0.0141	143.474	0.0131
133.599	34.811	140.026	0.0065	139.812	0.0064
132.576	34.342	135.326	0.0099	138.726	0.0088
138.157	34.758	166.346	0.028	165.778	0.0277
134.327	35.363	153.133	0.0051	146.469	0.0054
134.487	33.823	157.261	0.0263	160.343	0.0251
133.794	35.265	158.392	0.0044	141.841	0.0049
137.809	34.793	166.307	0.0275	164.45	0.0265
132.053	34.091	143.229	0.0104	143.978	0.0088
133.927	34.165	146.536	0.0155	146.966	0.0158
136.152	34.988	173.892	0.0166	178.351	0.0164
136.842	34.905	170.072	0.022	170.165	0.0221
133.657	33.768	150.79	0.0255	151.781	0.026
131.47	32.022	-179.716	0.0101	-167.838	0.01
132.938	33.57	153.514	0.0259	156.903	0.0266
135.168	35.294	161.011	0.0082	154.037	0.0079
132.704	32.841	153.5	0.0391	153.647	0.0386
132.014	34.572	136.172	0.0055	141.928	0.0057
131.61	34.618	133.514	0.0049	144.462	0.0047
135.025	35.24	163.28	0.0078	154.203	0.0078
135.84	33.521	168.693	0.0341	166.602	0.0357
131.334	32.385	-175.423	0.013	-173.937	0.014

132.909	34.635	138.414	0.007	136.684	0.0071
133.129	33.216	152.27	0.0372	152.252	0.0376
136.799	35.302	173.503	0.0186	174.184	0.0183
134.316	34.474	148.015	0.0089	150.203	0.0097
137.591	35.101	166.349	0.0228	169.512	0.0221
131.254	32.002	-156.817	0.0094	-156.479	0.0078
135.33	34.978	159.634	0.0099	165.401	0.0107
131.531	34.058	147.378	0.0079	148.157	0.0067
135.486	34.528	167.708	0.016	170.212	0.0156
132.922	35.494	121.091	0.0023	136.959	0.0039
136.873	34.985	170.858	0.022	170.666	0.0218
131.176	34.343	156.828	0.0057	148.669	0.0047
133.404	33.408	153.147	0.0356	151.278	0.0356
133.648	34.069	148.5	0.0178	148.463	0.0177
131.564	33.672	150.433	0.0116	151.888	0.0101
134	34.447	140.58	0.0089	145.24	0.0097
136.205	34.061	168.677	0.0251	166.902	0.0255
135.385	34.726	173.034	0.0139	169.796	0.013
132.996	35.197	137.657	0.005	137.141	0.0046
131.516	32.171	178.15	0.013	-178.34	0.0128
135.624	34.622	171.381	0.0161	172.184	0.0157
133.44	35.347	157.362	0.0048	138.618	0.0045
133.798	34.44	142.469	0.0102	142.87	0.0097
132.12	33.847	145.536	0.0138	145.265	0.012
134.378	34.762	156.446	0.007	154.527	0.0074
137.999	35.032	169.932	0.0238	170.142	0.0245
133.363	33.705	151.318	0.0251	153.028	0.0259
133.342	34.614	139.772	0.0082	137.624	0.0076
131.121	33.271	168.295	0.0097	164.277	0.01
136.638	34.432	169.252	0.0238	169.23	0.0244
138.642	35.203	177.439	0.0284	174.167	0.0292
138.094	34.94	167.427	0.0255	168.129	0.0259
132.694	33.447	166.717	0.0295	160.783	0.0271
132.974	33.313	153.544	0.033	154.561	0.033
132.475	33.385	156.25	0.025	162.553	0.0257
134.547	34.899	163.874	0.007	156.825	0.0074

136.351	34.209	169.201	0.0242	169.693	0.0241
132.54	34.68	150.442	0.0069	138.088	0.0063
134.864	34.494	156.06	0.0104	159.785	0.0112
135.559	33.942	169.226	0.0235	169.796	0.0232
133.19	34.253	141.66	0.0115	139.61	0.0116
132.821	34.336	142.615	0.008	137.629	0.0096
136.396	34.299	170.407	0.0237	171.774	0.0231
134.303	33.79	155.478	0.0275	157.123	0.0265
135.506	34.839	171.992	0.0126	170.278	0.013
131.757	32.704	163.553	0.0209	163.654	0.0226
135.877	33.8	172.601	0.0262	169.894	0.0275
135.176	34.688	166.04	0.0127	167.359	0.0116
134.948	34.938	157.97	0.0088	161.502	0.0089
133.701	35.492	135.554	0.0029	139.774	0.0043
138.065	34.666	165.212	0.0299	165.136	0.0313
137.053	35.129	167.977	0.0213	170.439	0.0215
132.903	35.037	152.024	0.0045	137	0.0051
132.104	33.976	146.798	0.0124	144.346	0.0102
132.686	34.858	142.984	0.0055	137.338	0.0056
138.4	34.99	169.848	0.0268	169.474	0.0256
135.711	34.699	174.631	0.0164	173.055	0.0156
134.167	34.659	155.283	0.0062	149.496	0.0076
131.357	33.538	155.018	0.011	156.591	0.0098
138.468	35.444	166.861	0.0249	172.642	0.0212
131.441	32.899	172.344	0.0179	174.608	0.0168
132.782	33.96	144.737	0.0158	142.038	0.0157
132.386	35.034	167.418	0.0047	138.512	0.0046
137.437	34.968	165.818	0.0238	167.344	0.0237
132.983	32.87	152.541	0.0413	152.891	0.0411
132.967	32.756	150.881	0.0424	151.716	0.0414
136.061	35.468	176.159	0.0113	171.384	0.0102
132.832	32.962	155.488	0.0388	154.089	0.0377
132.532	34.07	142.344	0.0128	140.864	0.0119
137.482	35.398	168.111	0.0186	168.563	0.0184
134.588	35.096	159.578	0.007	153.999	0.0069
133.532	33.627	151.315	0.0288	152.054	0.0294

138.101	35.045	171.559	0.0234	170.105	0.0255
137.137	35.48	172.128	0.0185	170.318	0.0164
136.401	34.856	173.707	0.0188	176.462	0.0185
136.07	35.321	172.771	0.0123	177.346	0.0124
135.749	34.157	171.555	0.0214	173.062	0.0204
132.824	34.573	136.5	0.0081	136.921	0.0074
136.603	35.229	177	0.0183	176.564	0.0184
138.197	34.849	167.103	0.027	166.82	0.0262
135.736	34.54	171.999	0.0194	173.331	0.0169
131.328	32.685	-176.904	0.0159	176.616	0.0154
136.559	35.373	174.77	0.0159	177.597	0.0158
135.614	35.464	166.938	0.0083	157.565	0.0078
132.793	33.172	155.083	0.0331	154.852	0.0335
136.839	35.191	170.552	0.0194	172.935	0.0199
131.629	32.853	171.692	0.0192	172.275	0.02
137.653	34.702	164.602	0.0279	162.043	0.0277
134.322	35.101	130.527	0.0083	150.501	0.0061
137.887	35.161	169.877	0.0228	171.667	0.0219
134.123	33.316	154.767	0.0452	153.072	0.0452
136.56	34.548	171.172	0.0223	172.481	0.022
136.017	33.742	167.332	0.0282	167.32	0.0308
135.779	35.054	174.172	0.0126	172.712	0.0128
136.704	35.052	172.324	0.02	173.509	0.0203
138.14	34.08	169.458	0.0497	161.4	0.0394
137.61	33.88	168.303	0.0493	162.218	0.0422
137.39	34.18	170.574	0.0513	173.493	0.0516
137	33.67	169.653	0.0362	171.425	0.038
136.67	33.43	166.896	0.0432	164.048	0.0404
136.36	33.33	165.161	0.0398	168.148	0.0394
135.57	33.16	159.545	0.0466	160.163	0.0455
134.94	33.35	163.591	0.034	160.607	0.0363
134.81	32.87	165.677	0.0388	166.005	0.0386
133.67	32.82	148.73	0.0545	149.146	0.0544
134.03	32.43	149.649	0.0481	150.022	0.0482
133.22	32.37	154.515	0.0451	154.755	0.0459
133.58	31.93	156.051	0.0421	153.463	0.0406

132.42	32.38	145.759	0.0375	146.819	0.0366
132.49	31.97	170.491	0.02	169.559	0.0205